universität wien

MASTERARBEIT | MASTER'S THESIS

Titel | Title

Assessing methane emissions from wetlands: A multi-model comparison and bias analysis in Canada and Scandinavia

verfasst von | submitted by

Lorenz Ferchländer BSc

angestrebter akademischer Grad | in partial fulfilment of the requirements for the degree of

Master of Science (MSc)

Wien | Vienna, 2025

Studienkennzahl lt. Studienblatt | Degree programme code as it appears on the student record sheet:	UA 066 299
Studienrichtung lt. Studienblatt | Degree programme as it appears on the student record sheet:	Masterstudium Environmental Systems: Processes - Pollution - Solutions
Betreut von | Supervisor:	Univ.-Prof. Mag. Dr. Andreas Stohl

Abstract

Methane, despite its much lower atmospheric concentration compared to CO_2, exerts the second largest radiative forcing of the major greenhouse gases due to its high heat-trapping efficiency. Wetlands constitute the single largest natural source of CH_4, yet as Saunois et al. (2019) show, uncertainties in wetland flux estimates are the dominant contribution to the overall methane budget uncertainty. These discrepancies undermine the reliability of climate projections.

To address this, we evaluated four wetland CH_4-flux scenarios: wetCHART, FLUXNET-CH_4, Poulter et al. (2017) and CAMS, by comparing their monthly emission fields over Canada and Scandinavia. We chose these two regions, because both contain extensive boreal wetland coverage alongside a relatively dense network of in situ CH_4 measurement stations. The four scenarios yield vastly different flux estimates: Canadian summer peaks reach up to $\sim$ 7 Tg (Poulter), yet the FLUXNET-CH_4 summer maximum of $\sim$ 2.2 Tg is only about 30 % of the Poulter et al. (2017) estimate. CAMS and WetCHART fall in between in both regions, whereas Scandinavian peaks vary by $\sim$50 % between the highest (Poulter) and the respective lowest scenarios.

Subsequently, we compared 2022 CAMS surface CH_4 concentrations against NOAA Obspack observations at East Trout Lake (ETL) and Behchoko (BCK) in Canada and Pallas (PAL) and Svartberg (SVB) in Scandinavia, subtracting the monthly median background signal from Alert (ALT) and Mace Head (MHD), respectively. These two stations were selected, based on a FLEXPART-derived footprint and source contribution analysis.

In Scandinavia, atmospheric mole fractions as simulated with the CAMS model have biases at PAL and SVB that range between –33 and +28 ppbv, without a clear seasonal pattern, reflecting the combined influence of wetland and anthropogenic sources, as well as influences from the subtraction of the background station´s seasonal pattern. Despite substantial deviations during individual months, background-corrected concentrations remain closely aligned with observations throughout the year (annual median bias < 2.2 ppbv), underscoring the CAMS model's high overall agreement with the observations in Scandinavia. Improving seasonal biases in this region will therefore require an effort to refine all prior emission sources, rather than targeting wetlands alone.

In contrast, wetlands dominate the regional emission landscape over Canada and

thus, for this region, the major part of the calculated biases and their seasonality can be attributed to wetlands. Here, background-corrected CAMS biases remain near zero through winter and increase during the active summer season, with annual medians of +8.65 ppbv at ETL and +28.67 ppbv at BCK. These findings reveal that the CAMS fluxes substantially overestimate wetland emissions during the peak season.

These results for Canada suggest that adopting lower-emission wetland priors during the active season could significantly mitigate summer overpredictions. From our wetland scenario-specific bias analysis, FLUXNET emerges as the most promising model to reduce summer model biases in Canada, whereas wetCHART (with an applied snow-cover mask to correct winter overestimates) exhibits biases slightly below those of CAMS and may also serve as a suitable emission prior for Canadian wetlands.

Zusammenfassung

Angesichts der rund 28 bis 34-fach höheren Treibhauswirkung gegenüber CO_2, trägt Methan (CH_4), trotz geringerer atmosphärischer Konzentration, nach CO_2 am zweitstärksten zum anthropogenen Strahlungsantrieb bei. Feuchtgebiete bilden dabei die mit Abstand bedeutendste natürliche Methanquelle. Die große Spannbreite heutiger Emissionsmodelle für Feuchtgebiete führt jedoch zu entscheidenden Unsicherheiten im globalen Methanbudget. Diese Unsicherheiten beeinträchtigen die Verlässlichkeit von Klimaprognosen.

Als ersten Schritt haben wir die vier Methanflussmodelle für Feuchtgebiete: wetCHART, FLUXNET-CH_4, Poulter et al. (2017) und CAMS über Kanada und Skandinavien ausgewertet und ihre monatlichen Flussfelder verglichen. Die vier Modelle sagen dabei stark unterschiedliche Emissionen voraus: In Kanada erreicht Poulter Höchstwerte von etwa 7 Tg CH_4 im Sommer, während FLUXNET nur ungefähr 30 % davon voraussagt und CAMS und wetCHART dazwischen liegen. In Skandinavien variieren die sommerlichen Emissionsgipfel um etwa 50 % zwischen dem stärksten Szenario (Poulter) und dem monatlich jeweils schwächsten Modell.

Danach haben wir die Abweichungen der CAMS-Modellkonzentrationen von den NOAA Obspack-Messwerten für die Messstationen BCK und ETL in Kanada, sowie PAL und SVB in Skandinavien, für das Jahr 2022 berechnet, nachdem wir zuvor die regionalen Hintergrundsignale (Alert (ALT) in Kanada; Mace Head (MHD) in Skandinavien) subtrahiert hatten. Diese vier Stationen wurden auf Basis einer FLEXPART-hergeleiteten "Footprint" und "Source Contribution"-Analyse ausgewählt. Wir haben uns für die Regionen Kanada und Skandinavien entschieden, weil beide Gebiete ausgedehnte boreale Feuchtgebiete aufweisen und über ein vergleichsweise dichtes Netz an in situ CH_4-Messstationen verfügen.

Für die skandinavischen Messstationen PAL und SVB liegen die hintergrundkorrigierten CAMS-Biaswerte zwischen etwa –33 und +28 ppbv, ohne ein klar erkennbares saisonales Muster. Trotz teils erheblicher Abweichungen in einzelnen Monaten stimmen die korrigierten Modellwerte über das gesamte Jahr hinweg sehr gut mit den Beobachtungen überein (jährlicher Median $< 2{,}2$ ppbv). Zur weiteren Minimierung verbliebener saisonaler Verzerrungen ist jedoch eine umfassende Überarbeitung aller zugrunde liegenden Emissionsinventare, nicht nur der Feuchtgebietsanteile, notwendig.

Im Gegensatz dazu prägen Feuchtgebiete das Emissionsbild in Kanada so stark, dass sich der Großteil der ermittelten Biaswerte und ihre Saisonalität auf die Feuchtgebi-

etsquellen zurückführen lässt. Nach der Korrektur des Hintergrundsignals liegen die CAMS-Biaswerte im Winter nahe bei Null, steigen aber im Sommer deutlich an und weisen jährliche Mediane von +8,65 ppbv an der Station ETL und +28,67 ppbv an der Station BCK auf. Diese Ergebnisse zeigen deutlich, dass das CAMS-Modell die Feuchtgebietsemissionen während der Sommerzeit, in der Feuchtgebiete aktiv sind, deutlich überschätzt.

Unsere Ergebnisse für Kanada zeigen, dass die Verwendung von emissionsärmeren Feuchtgebiet-Flussmodellen, bei der Modellierung von Methan-Konzentrationsfeldern, diese Überschätzung der Emissionen deutlich reduzieren kann. Unter den in dieser Arbeit untersuchten Modellen weist FLUXNET dabei den geringsten, sommerspezifischen Bias auf und erweist sich somit als besonders geeigneter Kandidat. WetCHART erzeugt Bias-Verläufe, die sehr eng an denen von CAMS liegen und bietet sich daher auch als brauchbares initiales Emissionsflussmodell für kanadische Feuchtgebiete an. Allerdings sollte hier eine Schnee-Maske zur Korrektur der Winterüberschätzungen angewendet werden.

Contents

1. General introduction: methane and wetlands

1.1. Methane as a greenhouse gas

Methane (CH_4) is the simplest alkane composed of a carbon atom and four hydrogen atoms. It is relatively stable, compared to other hydrocarbons, because it only forms strong, primary C-H sigma bonds. Methane has a relatively long atmospheric lifetime of about 9-12 years [35]. In comparison, other hydrocarbons like propane and butane, with more complex structures and weaker bonds, are more reactive, due to the lower activation energy of secondary or tertiary C-H bonds. Therefore, they have much shorter atmospheric lifetimes, typically days to weeks [1]. However, the lifetime of methane is significantly shorter than that of other greenhouse gases (GHGs) like carbon dioxide (CO_2), which can remain in the atmosphere for many centuries, or N_2O, which can last for over 100 years [33]. The primary atmospheric sink for methane is a reaction with hydroxyl radicals (OH), which leads to the formation of CO_2 and water vapour, which will be discussed in detail in section 1.3. Despite the shorter lifespan methane´s high radiative efficiency leads to a Global Warming Potential (GWP) of 28-34. This means that methane is 28-34 times more efficient at trapping heat than CO_2, over a 100-year period [35]. This trapping of heat in the atmosphere, or the greenhouse effect, enabled by greenhouse gases, such as water vapour (H_2O), carbon dioxide, methane, nitrous oxide (N_2O) or ozone (O_3) [38], is a natural effect on earth. A part of the solar radiation energy that is emitted into the atmosphere is reflected back into space, while the other part is absorbed by the earth´s surface and thereby warms it. The Earth then emits this energy back towards the atmosphere as infrared radiation. Subsequently, GHGs absorb and once again re-emit this infrared radiation towards the surface, which prevents the energy from leaving the climate system, thereby essentially warming the earths lower atmosphere and surface. The absence of this effect would lead to an average surface temperature of only around -18°C, making it unhabitable for human life [41].

Methane is released into the atmosphere through natural and anthropogenic processes. Natural sources include wetlands, termites, oceans, wildfires and geological releases [34], while the main anthropogenic sources are agriculture, waste industries and the extraction and burning of fossil fuels [35, 28], as highlighted in figure 1.1.

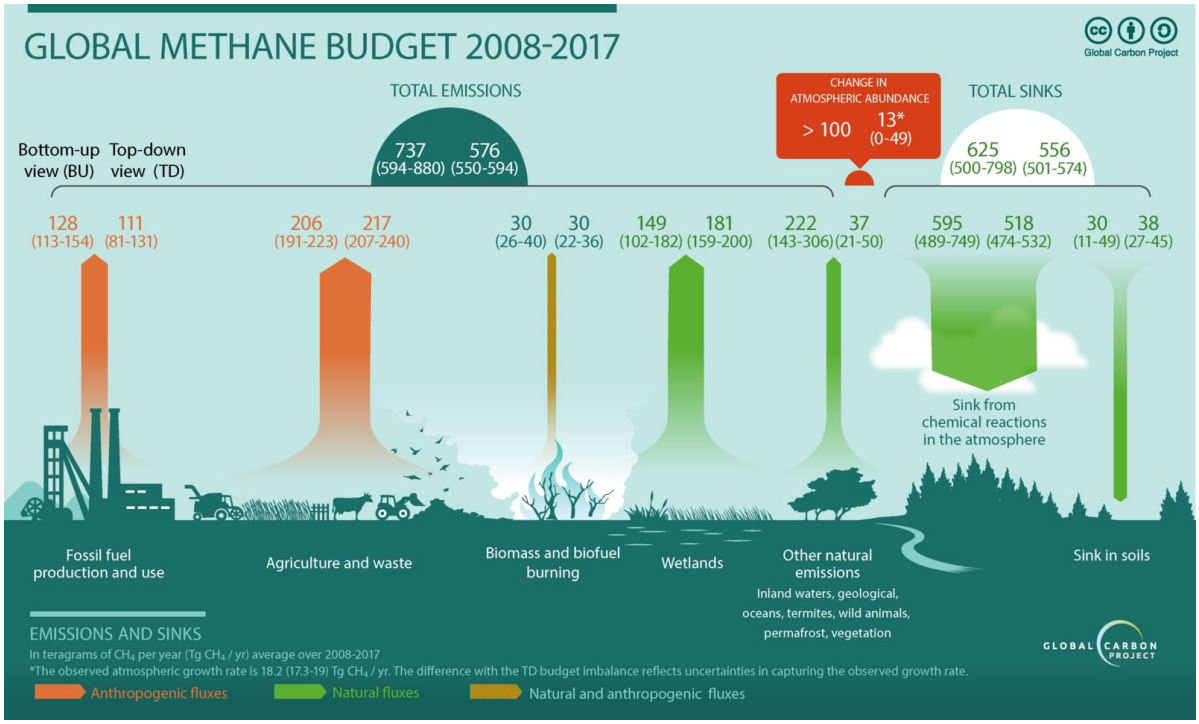

Figure 1.1.: The annual sources and sinks of global methane emissions and their respective concentrations in Tg CH_4 per year, averaged over the years 2008-2017, taken from Saunois et al. (2019) [35].

Figure 1.1 shows the methane budget averaged over the years 2008–2017. The various sources and sinks and their corresponding concentrations in Tg/yr are depicted for both bottom-up (BU), as well as top-down methods (TD). Bottom-up methods estimate methane fluxes by collecting surface emission data from individual sources, which are then scaled using empirical factors or process-based models to generate regional or global datasets. In contrast, top-down methods, use atmospheric measurement data and trace these concentrations back to their surface emission sources, using atmospheric transport models and inverse modelling techniques. Wetlands represent the largest natural source of methane emissions globally, as depicted in figure 1.1. However, they are also a major source of uncertainty, due to large differences between wetland models, as well as between top-down and bottom-up estimates. A more detailed explanation and a few examples are given in section 2.1. Saunois et al. (2019) [35] point out that

a more accurate distinction between methane emissions from wetlands, freshwater systems, and thawing permafrost could be crucial for aligning top-down and bottom-up estimates of natural sources. Furthermore, developing models that accurately depict the global wetland methane budget with minimal bias against observations is essential to laying the groundwork for timely and effective climate action. Therefore, we conduct a broad regional analysis of wetland methane emissions in this study, rather than assessing fine-scale spatial fidelity.

1.2. Wetlands as a source of methane

According to Saunois et al. (2019) [35], wetlands are "ecosystems with inundated or saturated soils or peats where anaerobic conditions lead to methane production." The term "wetland" contains a variety of ecosystems characterized by their hydrology, nutrient inputs and vegetation. The main wetland categories are marshes, swamps, floodplains, mangroves and peatlands. The latter are water flooded all year and plant material decays under the acidic, anoxic conditions, which is then called peat. Peatlands can be separated into two types: bogs, which contain nutrient poor and acidic rainwater and fens, with less acidic nutrient rich groundwater. Between 2008 and 2017 wetlands contributed a median estimation of 161 Tg CH_4 yr^{-1} (125–218 Tg yr^{-1}), representing roughly 20–35 % of atmospheric inversion (top-down) budgets and 15–30 % of bottom-up totals [35]. From the latitudinal analysis of global wetland emissions, Saunois et al. (2019) conclude that $\sim$ 65% of the emissions stem from tropical regions below 30 °N, around 30% between 30 - 60 °N and the remaining 5% from boreal and Arctic regions above 60°N [35].

Precisely quantifying CH_4 emissions from wetlands remains a huge challenge. Wetlands exist in various forms, each with its own characteristics and dominant methane production pathways. In any modelling approach, it is immensely challenging to fully capture the complexity of the various methane emission pathways, as described below in section 1.3. For accurate results a range of parameters need to be integrated into the modelling framework, from the biochemistry of CH_4 release from wetlands to the dynamics of wetlands and their key predictors (environmental parameters). Furthermore, uncertainty in defining the extent of wetlands worldwide contributes to uncertainties in estimating total methane emissions and the often insufficiently accurate separation from freshwater systems, such as lakes and rivers, can lead to under or double-counting of emissions in many datasets [26].

Nevertheless, the accurate quantification of wetland emissions is crucial because of their substantial impact on atmospheric methane levels. Understanding and accurately estimating methane emissions is vital for climate change mitigation. The quantification of the CH_4 fluxes is done via biochemical models and the quality of the emission estimates heavily relies on those especially for bottom-up, but also for top-down models. This will be further discussed in section 2.1. Given the significant contribution of wetlands to natural CH_4 sources, constant improvements need to be facilitated, in order to reduce the uncertainty of the contributions of wetlands to the global methane budget.

1.3. The chemistry of methane in wetlands and the atmosphere: an overview

The aim of this chapter is to provide a brief and simplified overview of the biochemistry of methane in wetlands and to highlight the major chemical processes and the environmental factors they depend upon, in order to get an overarching understanding of how methane is produced and released in wetlands.

1.3.1. Methane emission pathways

In wetlands, most of the CH_4 is produced by methanogenic archaea (methanogens). Under the water-flooded anaerobic conditions, fermentation processes, mostly facilitated by bacteria, produce substrates used by methanogens. The most prevalent substrates in most wetlands are acetate (CH_3COOH) and CO_2. Bridgham et al. [9] state that more than 90 % of methane produced in freshwater wetlands arises from one of two processes:

Acetoclastic methanogenesis

In this pathway, methanogens take up acetate (CH_3COOH) into their cells and use enzymes to split it into CO_2 and a methyl group CH_3, which is subsequently enzymatically reduced to methane:

$$CH_3COOH \longrightarrow CH_4 + CO_2.$$

This pathway predominates in environments where fermentative bacteria supply high concentrations of acetate, such as fens [21].

Hydrogenotrophic methanogenesis

In this pathway, methanogens take up carbon dioxide (CO_2) and hydrogen (H_2) into their cells. In simplified terms, enzymes called hydrogenases split the covalent bond in

H_2 molecules, releasing electrons, which reduce CO_2, yielding methane (CH_4) and water (H_2O).

$$CO_2 + 4\,H_2 \longrightarrow CH_4 + 2\,H_2O$$

This mechanism is dominant in acidic environments, such as bogs, where enough H_2 and CO_2 are present [9].

Once methane molecules are produced, there are a few main scenarios in which CH_4 can be emitted from wetlands into the atmosphere: Firstly, diffusion through the inundated soil along concentration gradients. However, during this slow process, CH_4 can pass through oxic layers near the surface, where aerobic methanotrophic bacteria typically oxidize large fractions (up to 90%) of the methane to CO_2 and H_2O before it ever reaches the atmosphere [22]. Secondly, via ebullition, the release of methane in the form of gas bubbles from waterlogged soils. If methane production happens faster than it can diffuse away or be oxidized in certain areas, these areas become saturated with CH_4 and gas bubbles start to form, which then quickly rise to the surface and thereby release methane directly into the air, without oxidation. Lastly, via the transport through plant aerenchyma. In this process, methane can rise to the atmosphere directly from the soil, through the roots and porous aerenchymous tissues of plants within the wetland, bypassing oxidation [21]. All of the processes above are schematically depicted in figure 1.2.

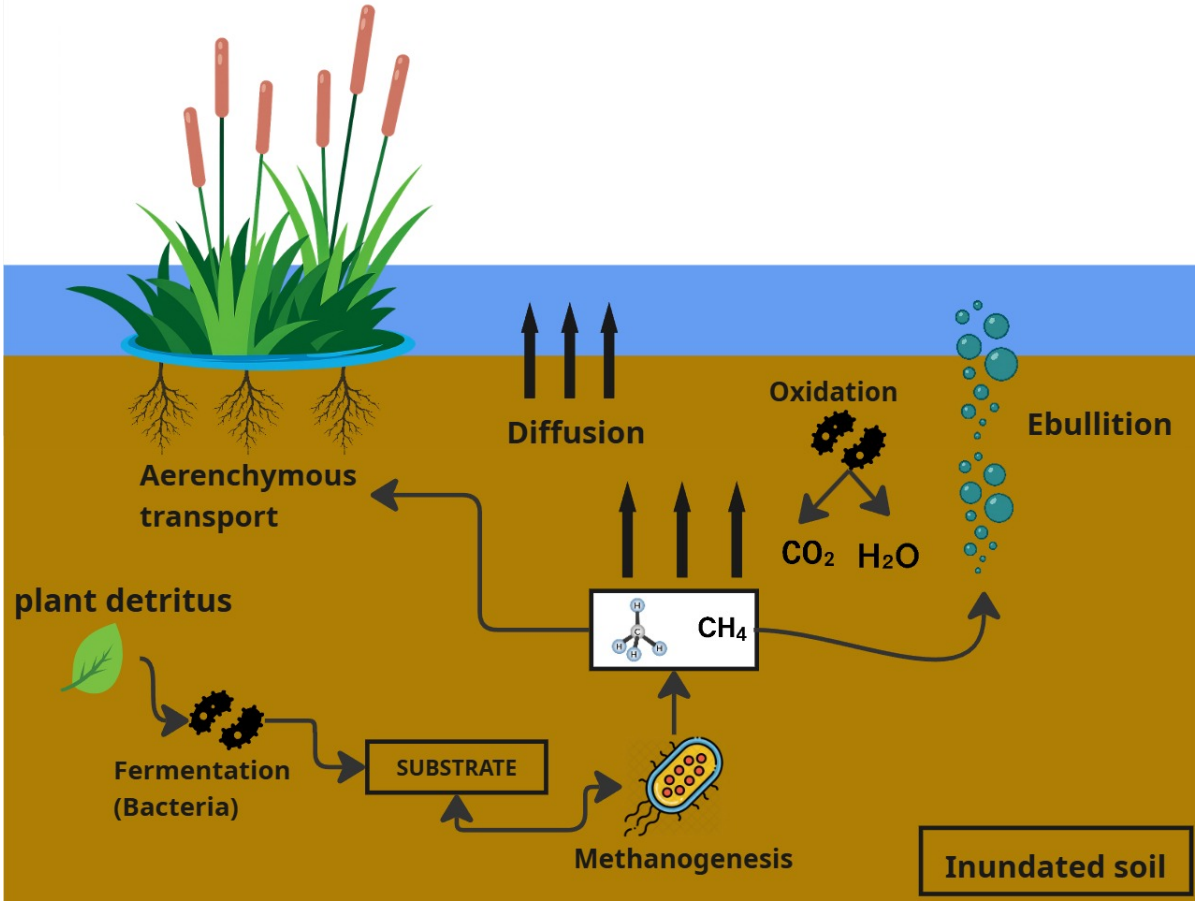

Figure 1.2.: A simplified schematic illustration of the key chemical reactions and pathways, regarding the production and release methane in wetlands.

1.3.2. Key emission drivers

Despite the high level of complexity and the multitude of variables in capturing CH_4 fluxes from wetlands, the main drivers for the release of methane from wetlands can be divided into three categories: water table depth, soil temperature and the type of vegetation present [20, 40].

Water-table depth The depth of the water table demarcates the boundary between oxic and anoxic conditions and thereby determines the overall volume available for methane production and release. A decreasing water table means that more soil volume remains under aerobic conditions, which reduces the net CH_4 emissions and vice versa. Turetsky et al. (2014) found that the water level describes the largest part of emission variabilities for most of the examined 71 wetlands in both subtropical and northern regions [40]. However, methane emissions do not increase indefinitely with rising water

tables, but reach an optimum. Beyond this optimal water level, an increase in water level even reduces the speed of CH_4 release. Diffusion is slowed, because the methane molecules need to travel through a thicker water layer and the increase in hydrostatic pressure hinders the formation and rise of gas bubbles, thereby reducing ebullition [42].

Soil temperature Soil temperature influences the metabolic rates of both the substrate production via fermentation, as well as the production of methane by methanogens. Therefore, the soil temperature directly correlates with the release of methane, which leads to higher emissions during warmer months [20]. This predictor was found to be the second largest factor in explaining the wetland emission variability by Turetsky et al. (2014) for most wetland types. More precisely, they found that an increase of 10°C nearly doubles the methane production rate across all examined wetland sites [40].

Vegetation type

Here, vegetation type refers to the composition and structure of the plant and microbial communities. Although water table depth and soil temperature are the primary controls on CH_4 emissions in many wetland types, such as bogs and swamps, this can change for other wetlands. For instance, Turetsky et al. (2014) showed that for pristine, Carex-dominated fens, plant-mediated CH_4 transport through aerenchyma explained the dominant part of emission variations.

1.3.3. The atmospheric fate of methane

Once methane is emitted, almost the entire removal of CH_4 in the atmosphere can be condensed into a few key reactions. The largest sink is the reaction with hydroxyl radicals (OH), which makes up $\sim 90\%$ of the total atmospheric CH_4 loss.

In the lower atmosphere, mainly in the troposphere, CH_4 reacts with OH to form methyl radicals and water vapour:

$$CH_4 + OH \longrightarrow CH_3 + H_2O.$$

OH radicals themselves are produced when UV sunlight photolyses O_3 to generate excited oxygen atoms $O(^1D)$, which then react with H_2O. This reaction controls the atmospheric lifetime of methane and contributes to tropospheric ozone formation [35, 24].

In the stratosphere, CH_4 is also oxidized by chlorine and excited oxygen via the reactions:

$$CH_4 + Cl \longrightarrow CH_3 + HCl$$

$$CH_4 + O(^1D) \longrightarrow CH_3 + OH.$$

Together, these processes remove around 31 Tg CH_4 per year from the atmosphere [35]. Furthermore, OH radicals are regenerated during methane oxidation, which leads to an effectively self sustaining cycle that continuously removes methane [24].

As previously mentioned, atmospheric CH_4 can also be oxidized via aerobic methanotrophic bacteria in soils. In this process methane is oxidized stepwise to CO_2, which removes ∼30 Tg of CH_4 per year [35], comparable to the chlorine uptake.

Importantly, wetlands can switch roles depending on the overall circumstances: when soils are waterlogged, anaerobic conditions lead to a release of methane. However, when these areas dry out, so that parts of the soil experience more aerobic conditions, these methanotrophs can get activated and consume CH_4, which can turn a wetland from a source into a net sink and vice versa.

2. Methods

This thesis evaluates and compares four different wetland CH_4 emission scenarios. These include the bottom-up models wetCHART, FLUXNET-CH_4, and the Poulter et al. (2017) ensemble, as well as the top-down inversion product from the Copernicus Atmosphere Monitoring Service (CAMS) for methane [4, 32, 11, 6]. Each of these datasets provides monthly-resolved methane fluxes at a global scale, but they differ substantially in their input data, methodologies, and assumptions. By analysing and comparing their spatial and seasonal emission patterns, we aim to assess their respective strengths and limitations, and to explore how the choice of flux scenario can influence modelled atmospheric methane concentrations, thereby identifying potential avenues for future research. Furthermore, we study CH_4 concentrations over wetland-dominated regions by analysing global concentration fields provided by CAMS [4]. Moreover, we evaluate the influence of wetland emissions on the modelled concentrations using FLEXPART-Source Receptor Relationship simulations. To evaluate the performance of the modelled concentrations, we compare the CAMS data with independent in-situ measurements. This comparison allows us to assess the model bias and how well the modelled CH_4 fields capture the overall emissions and their seasonality.

2.1. Wetland scenario models

Direct measurements of methane emissions can be insightful, but face inherent limitations. Ground-based eddy covariance measurement stations cover only localized areas, and satellite data often have spatial gaps or are affected by atmospheric conditions like cloud cover. These constraints hinder our ability to fully capture the complexity of wetland methane emissions, which vary significantly across regions and seasons.

Surface flux models address these gaps by simulating methane emissions based on environmental parameters, such as temperature, soil moisture, and vegetation dynamics, providing global coverage and the ability to predict emissions under different conditions. Although models are typically tested and optimized towards eddy covariance

measurements, each model employs distinct assumptions and methodologies, leading to variability in predictions. To highlight the diversity in model structures and outputs, we briefly introduce four representative models with notably different approaches:

wetCHART (bottom-up): An estimate for CH_4 emissions from wetlands can be modelled using the wetCHART framework. Calculations utilise the following factors: a global scaling factor (s), wetland extent fraction ($A(t,x)$), carbon heterotrophic respiration per unit area ($R(t,x)$), and the temperature (T) dependent ratio of carbon respired as CH_4 ($q_{10}^{T(t,x)/10}$).

$$F(t,x) = sA(t,x)R(t,x)q_{10}^{T(t,x)/10}. \tag{2.1}$$

Depending on the specific case, wetCHART models estimate these components using various biochemical models [6]. In this work we use the wetCHART v1.3.1 dataset from Bloom et al. (2021) [7], where $R(t,x)$ is taken from an ensemble of nine terrestrial carbon-cycle simulations (eight MsTMIP land-surface models and one CARDAMOM inversion), $A(t,x)$ is estimated by combining static wetland extent maps (ESA GLOBCOVER or GLWD) with dynamic scaling factors based on either SWAMPS multi-satellite inundation or ERA5 precipitation, $q_{10}^{T(t,x)/10}$ is computed using three literature-based temperature-sensitivity parameterisations applied to ERA5 surface skin temperature, and s is chosen per configuration to calibrate each member's global annual CH_4 flux to a reference budget. The wetCHART dataset allows you to select among different model configurations via a four digit code, one digit for each term in equation 2.1. In this work, we used the "0000" configuration, meaning the first entry for all four components.

FLUXNET-CH4 (bottom-up): FLUXNET-CH4 fluxes are assessed from eddy covariance measurements that sample vertical wind speeds and CH_4 concentrations at a high frequency. Fluxes are estimated by averaging the covariance of deviations in vertical wind (w') and CH_4 concentration (c') over fixed intervals, yielding

$$F = \overline{\rho\, w' c'}\,,$$

where ρ is the air density. After routine quality control and gap-filling to address data gaps, these half-hourly fluxes are aggregated and extrapolated spatially and temporally to produce the global FLUXNET-CH4 dataset [11]. Here, we used their data product version 04 for 2018.

Poulter et al. (2017) (bottom-up): Poulter et al. [32] employed an ensemble of eleven process-based models to estimate monthly global wetland CH_4 emissions for

2000–2017. Each model was driven by the same set of inputs: daily inundation maps from SWAMPS (bias-corrected to match the total wetland area in GLWD), meteorological data from the CRU-NCEP reanalysis, and a set of atmospheric CO_2 concentration data. Simulations were performed on a uniform 0.5° x 0.5° grid, and the emission estimate was calculated via the ensemble mean. This methodology provides a methane flux dataset in which the dependence on any single individual model assumption is minimized. Hereafter, whenever we use "Poulter" in this thesis, we are referring exclusively to this Poulter et al. (2017) dataset. In figures, legends and text we simply abbreviate it as "Poulter" for better readability.

CAMS (top-down): In this thesis we use the latest CAMS Global Greenhouse Gas Inversion surface flux data for 2018, which produces monthly wetland CH_4 emission maps by combining a process based ecosystem simulation with atmospheric methane measurements. The ecosystem simulation is performed by LPJ-DGVM (the Lund–Potsdam–Jena Dynamic Global Vegetation Model), which, driven by daily temperature and precipitation inputs from the CRU dataset and MERRA2 reanalysis, models carbon cycling across plant functional types and tracks the fraction of each grid cell that becomes waterlogged, thereby capturing the extent of anaerobic soils, in which methane is produced. The emissions from the ecosystem model fluxes are then adjusted to better fit the atmospheric measurements. Furthermore, these emission fluxes are used as a priori emission fields for the TM5 chemistry–transport model (run on a 1° x 1° grid with ERA-Interim meteorology reanalysis data, produced by the European Centre for Medium-Range Weather Forecasts (ECMWF)). This model then simulates how methane moves and is removed in the atmosphere to produce concentration fields based on these priors. To minimise the divergence of simulated and observed CH4 concentrations, a four-dimensional variational inversion (4DVar) is applied to the TM5 model. This iteratively refines the flux fields by adjusting fluxes across three spatial dimensions and time, hence "four-dimensional" [5]. This procedure produces monthly global CH_4 concentration maps, which we are going to compare against measurement data in section 3.2.

In summary, WetCHART combines multiple individual data inputs to capture biogeochemical dynamics at high resolution, but its results are strongly dependent on the chosen wetland maps, respiration models and the global scaling factor. FLUXNET-CH_4, on the other hand, delivers direct, high-frequency measurements, grasping short-term variations, but it is limited by the spatial distribution of eddy-covariance measurement stations and thus need extrapolation to the spatial extent of the wetlands. The Poulter et al. (2017) dataset averages over eleven process-based models, reducing the biases of

any single model, but all of the eleven models are driven by the same meteorological and wetland data. Thus, uncertainties in these data are propagated through every model, before the ensemble averaging.

In contrast, CAMS employs a top-down inversion framework that uses atmospheric methane observations as inputs for an atmospheric transport model, providing an emission grid with global coverage, where the emission patterns are consistent with measurement data. However, it heavily relies on the accuracy of the transport model and might miss regional details, such as smaller wetlands.

Overall, bottom-up methods (wetCHART, FLUXNET-CH_4 and Poulter et al. (2017)) excel at process detail and local accuracy, but their output is highly dependent on the accuracy of parameter choices and the necessary data in each case. The top-down CAMS inversions ensure consistency with atmospheric observations, by optimizing the biochemical models towards measurements. However, the inversion process needs a priori emission fields from biochemical (bottom-up) models, so any biases or spatial patterns in those priors will carry through into the optimized flux estimates. In addition, they might lack fine regional details and rely on transport model accuracy. An abbreviated summary of the key principles and the strengths and weaknesses of the four models is shown in table 2.1 below.

Table 2.1.: Key features of the four wetland CH_4 flux scenarios.

Model (year)	Type	Key Principle	Strengths	Limitations
wetCHART v1.3.1 (2018)	bottom-up	Estimate CH_4 release via formula in 2.1	captures biochemical details	dependent on maps used in formula
FLUXNET-CH_4 (2018)	bottom-up	Aggregates eddy-covariance CH_4 flux measurements into monthly global fields.	direct, high-frequency	needs extrapolation
Poulter et al. (2017)	bottom-up	Averages an ensemble of 11 process-based wetland models driven by inundation and climate data.	reduces single-model bias	shared driver data uncertainties in output
CAMS Inversion (2018)	top-down	Optimizes LPJ-DGVM fields via 4D-Var to match atmospheric CH_4 observations	more consistent with observations	relies on accuracy of a priori fields and transport model

2.2. Atmospheric measurement data

To validate the CAMS-simulated surface-level CH_4 mixing ratios (see section 2.1), we compared them against independent in situ measurements from the NOAA Obspack data product (v06) for 2022 [36]. The data package comprises 530 atmospheric methane datasets compiled from measurements conducted by 67 laboratories worldwide, covering the period from 1983 to 2023, including aircraft and various in-situ surface measurements. The diversity of this package, collected from numerous independent sources, makes this dataset well suited for validating and comparing modelled atmospheric methane concentrations. We limit our validation to Obspack measurements taken at altitudes below 1000 m to ensure comparability with the CAMS surface-level concentrations and because the wetland emissions are not captured by higher stations in mountains.

2.3. FLEXPART: Source Receptor Relationship (SRR)

FLEXPART is a Lagrangian particle dispersion model used for simulating atmospheric transport processes. It releases virtual particles into the atmosphere and tracks their movement based on meteorological fields, providing insights into the dispersion of pollutants, aerosols, or GHGs, such as methane. It utilizes 3D gridded meteorological fields to calculate particle trajectories, including wind velocities, pressure, specific humidity, or temperature. As the particles move, FLEXPART simulates various processes such as gravitational settling, dry deposition, and wet deposition to calculate the trajectory of these particles and their mass changes [31]. There is also a Linear Chemical Module (LCM) within the FLEXPART framework, which extends the model´s capabilities to simulate linear chemical reactions and the transport of multiple chemical species [2] in a global domain-filling setup. Moreover, FLEXPART can run both forwards in time, predicting where a pollutant released from any given source will go, and backwards, determining which surface areas contributed to measured concentrations at a given station and time. We used the latter feature in this thesis to gain knowledge about the contributions of wetlands to observed concentrations. This is also called the source receptor relationship (SRR). FLEXPART calculates this relationship, by releasing a large ensemble of virtual particles from the sampling height and location of a given station and traces their trajectories back through meteorological wind fields. For the SRR calculations, we released particles in three-hour intervals to obtain footprints at a three hour resolution and averaged all CH_4 measurements over this time interval. The model tracks how long each particle remains within every grid cell in the lowest 100 m for a chosen intervals of 600s and over the entire duration of the backwards simulation, those residence times are summed and averaged over all particles, yielding a sensitivity value for each cell, in the unit of m^3s/kg. By multiplying the emission sensitivity with the emission fluxes in each cell, FLEXPART quantifies how emissions in each location contribute to the concentration measured at the station [37].

For this thesis, 15 000 virtual particles were released in each averaging window and we used hourly 0.5°x0.5° wind fields from the ERA5 reanalysis dataset by ECMWF for our backwards simulations [15]. We calculated the inverse trajectories for 15 days and the chemical interactions were neglected, because methane has a lifetime of around 9-12 years in the atmosphere and during these 15 days only a negligible part of methane would have been lost due to oxidation by OH radicals. This combination of parameters

has proven to be a viable compromise in providing sufficient information, while reducing computational time as much as possible.

For Canada we examined the inverse trajectories of these measurement stations: Fraserdale boreal forest site (FRD) and East Trout Lake (ETL) in Saskatchewan and a station near Behchoko (BCK) in the North West, surrounded by mixed forests, lakes and ponds. In Scandinavia we looked at the Finnish station Pallas (PAL), which lies amid wetlands, lakes and scattered forest patches, Svartberg Atmospheric Station (SVB) in a Swedish boreal forest and Puijo Station in Finland (PUI). [43].

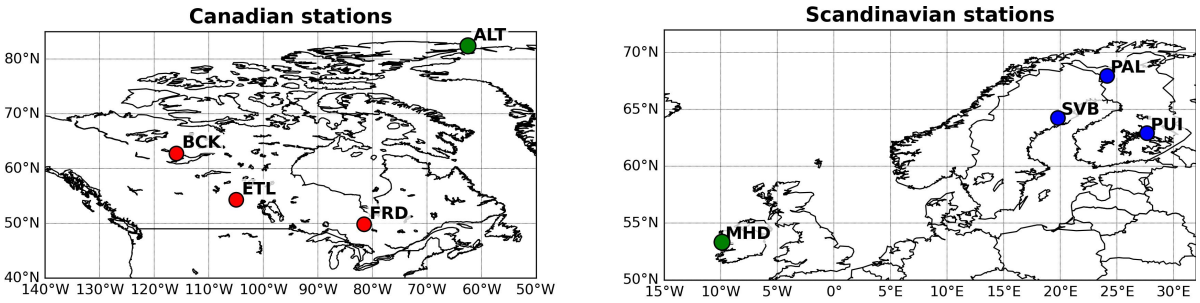

Figure 2.1.: Locations of the measurement sites used for the FLEXPART backwards simulations. The left side shows the stations BCK, ETL and FRD and the background station ALT in Canada and the right side shows the stations PAL, PUI and SVB and the background station MHD in Scandinavia.

The locations of the observation sites are illustrated in figure 2.1. We chose these stations, because they measure in areas, where the wetland flux emissions show high values and a strong seasonality (see fig.3.1).

3. Results and Discussion

3.1. Analysis of wetland fluxes

3.1.1. Wetland scenario CH_4 flux comparison

Firstly, we conducted a preliminary analysis of the global fluxes to gain an overarching view of the methane emission landscape and to explore wetland model uncertainties, by comparing all the discussed wetland scenarios in section 2.1. The global emissions are depicted in figure 3.1, averaged over four summer (May-Aug) and winter months (Nov-Feb), to achieve decent visibility, while capturing seasonal patterns. Although the maximum flux values were higher in each scenario, ranging from $\sim$ 3 - 3.5 10^{-9} kg/m^{2}s, we capped the colour scale at 10^{-9} kg/m^{2}s in all panels to enhance the visibility of regional variations in the lower-to-moderate flux areas that would otherwise be overshadowed by high emission areas. Although we later use CAMS concentration data from 2022, the flux data from 2018 (and 2017 for Poulter et al. (2017)) was chosen to match the available output years of the wetland models and to ensure consistency across scenarios. This approach is justified, because the differences between models are much larger than those between individual years, making the selected years suitable for comparison [44].

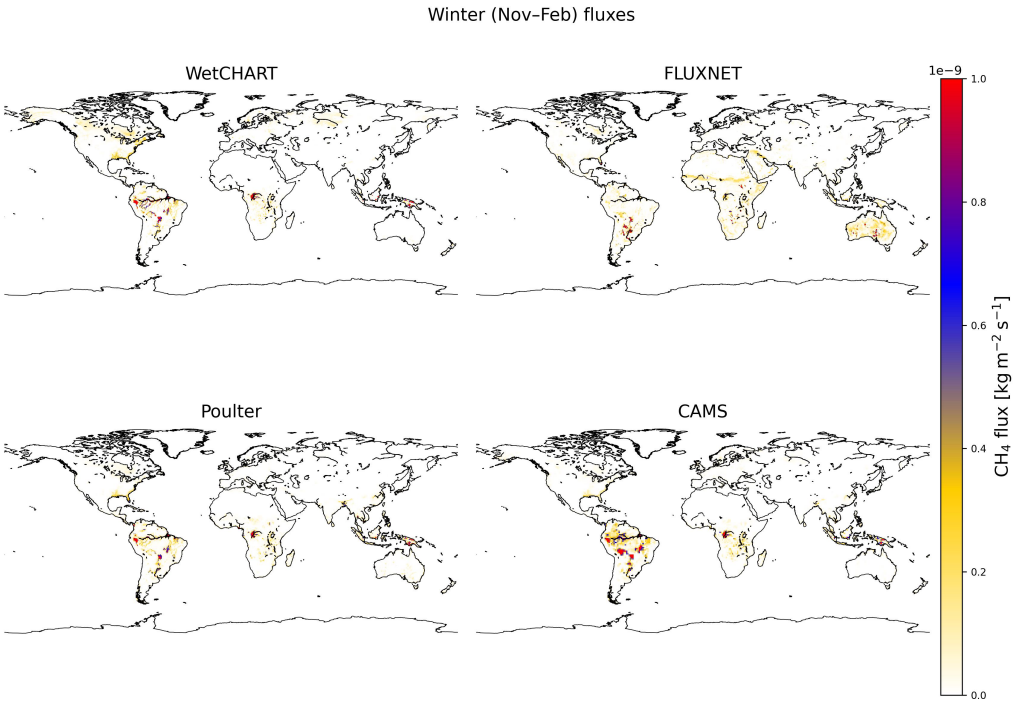

(a)

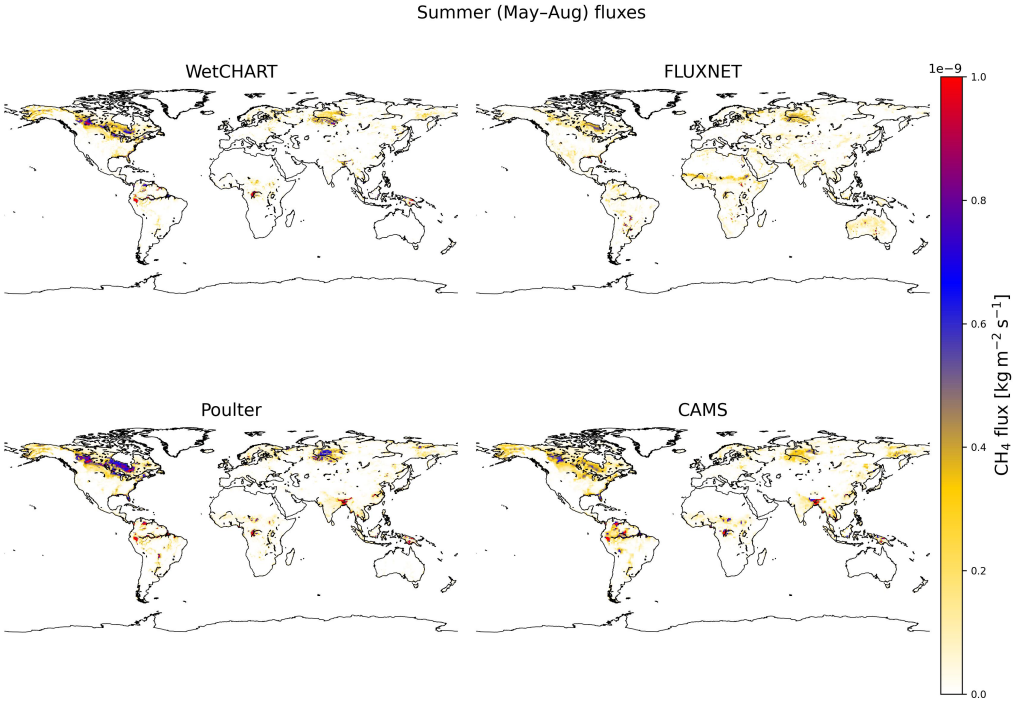

(b)

Figure 3.1.: Seasonal mean wetland CH_4 fluxes in kg/m^2 s for (a) winter (Nov–Feb) and (b) summer (May–Aug) averages, across the four emission scenarios: wetCHART, FLUXNET, Poulter et al. (2017), and CAMS. All maps share a colour scale capped at 10^{-9} kg/m^2 s.

Figure 3.1 demonstrates that all four wetland emission scenarios (CAMS, Poulter et al. (2017), wetCHART and FLUXNET) contain the same broad spatio-temporal patterns: tropical basin wetlands in the Amazon, Congo and Southeast Asia dominate methane fluxes over the course of the whole year with only modest seasonal changes. On the other hand, northern boreal wetlands (e.g. Canada, Scandinavia) are essentially inactive in the winter months and peak in the warm summer months. Southern and mid-latitude regions, such as Australia or more southern parts of South America or Africa, follow similar but lower amplitude cycles. Emissions in the Southern Hemisphere peak during November-February and have minimal values in May-August. These patterns are consistent with established knowledge of global methane fluxes [35]. Emissions are usually higher in warmer and wetter periods and lower during colder or drier times, as described in section 1.3.2. While all four scenarios reproduce the same broad seasonal cycle, they visibly differ across various factors, such as the wetland extent, the flux amplitudes and their emission coverage. For example, the seasonal cycle of Australia, is only covered by the FLUXNET dataset. For Canadian wetlands, WetCHART and Poulter et al. (2017) sharply delineate known wetland areas, while CAMS produces a more diffuse emission field and FLUXNET records even less detailed emissions.

Following this initial global assessment, we chose to focus our regional analysis on Canada and Scandinavia throughout the entire thesis. These regions contain a relatively high density of in situ measurement sites, compared to other regions, which provides a strong observational basis for a comparison with modelled concentration data later on.

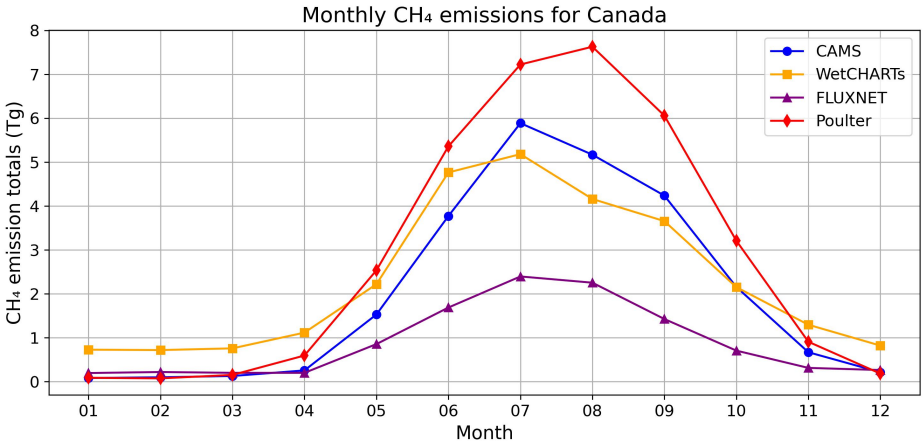

(a)

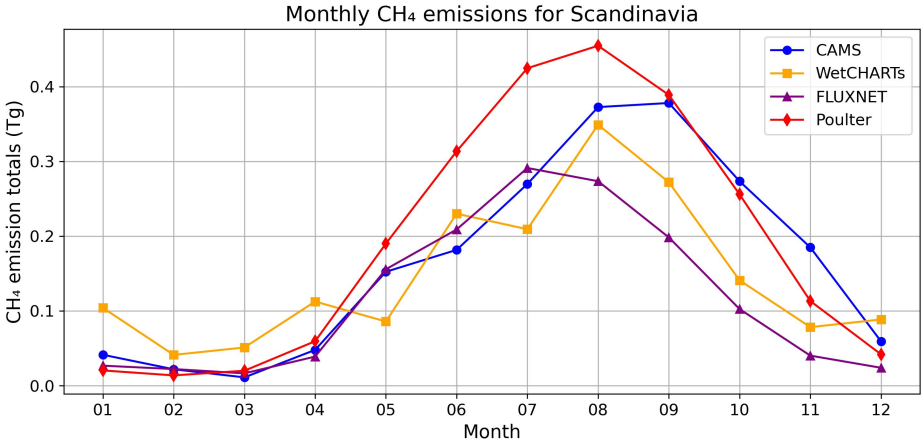

(b)

Figure 3.2.: Total methane emissions per month in Tg for different wetland scenarios over Canada (a; 35°–75° N, –150° to –40° E) and Scandinavia (b; 54°–72° N, 0°–35° E).

Notably, our chosen areas (35°–75° N, –150° to –40° E for Canada; 54°–72° N, 0°–35° E for Scandinavia) extend beyond national borders and include parts of the ocean and other countries. They were deliberately defined this broadly to ensure that all wetland areas within each region are captured, but as a result the plotted totals also encompass emissions from neighbouring countries. However, since our goal is to compare model outputs, the precise delineation of the emission regions is not of importance here. The extent of these bounds is shown below in figures 3.3 and 3.4.

Figures 3.2(a) and 3.2(b) present a comparison of monthly emission totals derived from the previously introduced wetland CH_4 emission models WetCHART, FLUXNET,

Poulter et al. (2017) and CAMS for Canada and Scandinavia. As can be seen in figure 3.2(a), for Canada the emission totals can vary up to $\sim$ 5 Tg in the summer months. Here, Fluxnet estimates only $\sim$ 30 % of the Poulter et al. (2017) emissions. For Scandinavia, as illustrated in figure 3.2(b), differences are smaller, but summer and autumn emissions can still differ by up to $\sim$ 50%, meaning the lowest respective estimates predict only up to about 50% of the highest (Poulter).

The comparison of different wetland scenarios emphasises not only the often drastic model divergence, but also introduces the possibility of choosing appropriate wetland emission priors when constructing CH_4 concentration fields. Identifying which model performs best under specific regional and seasonal conditions may significantly improve the accuracy of atmospheric CH_4 simulations and thus represents a valuable avenue for further research.

3.1.2. WetCHART snow cover analysis

A notable feature of the wetCHART dataset is that it estimates higher emissions during the winter months, likely as a result of WetCHART applying a temperature-sensitivity scaling factor q_{10} to all inundated grid cells throughout the whole year, as shown in equation 2.1. However, if soil is covered in snow or ice, the diffusive gas transport is considerably reduced, leading to the trapping of methane gas below the snow and ice layers [30]. Therefore, we examined the monthly-averaged snow cover data from the ERA5-Land reanalysis [27] for 2022 and compared them to the WetCHART fluxes for both regions.

Figures 3.3 and 3.4 present a comparison of the mean methane fluxes (left column) with snow-cover fraction (right column) for Canada and Scandinavia for the months of January, April and December. We chose these months to examine winter months, during which wetCHART estimates higher emissions than the other wetland scenarios. Additionally, we added April, because wetCHART still estimates higher emissions than the other models here (see fig. 3.2) and to roughly examine how the snow cover changes during the warmer spring.

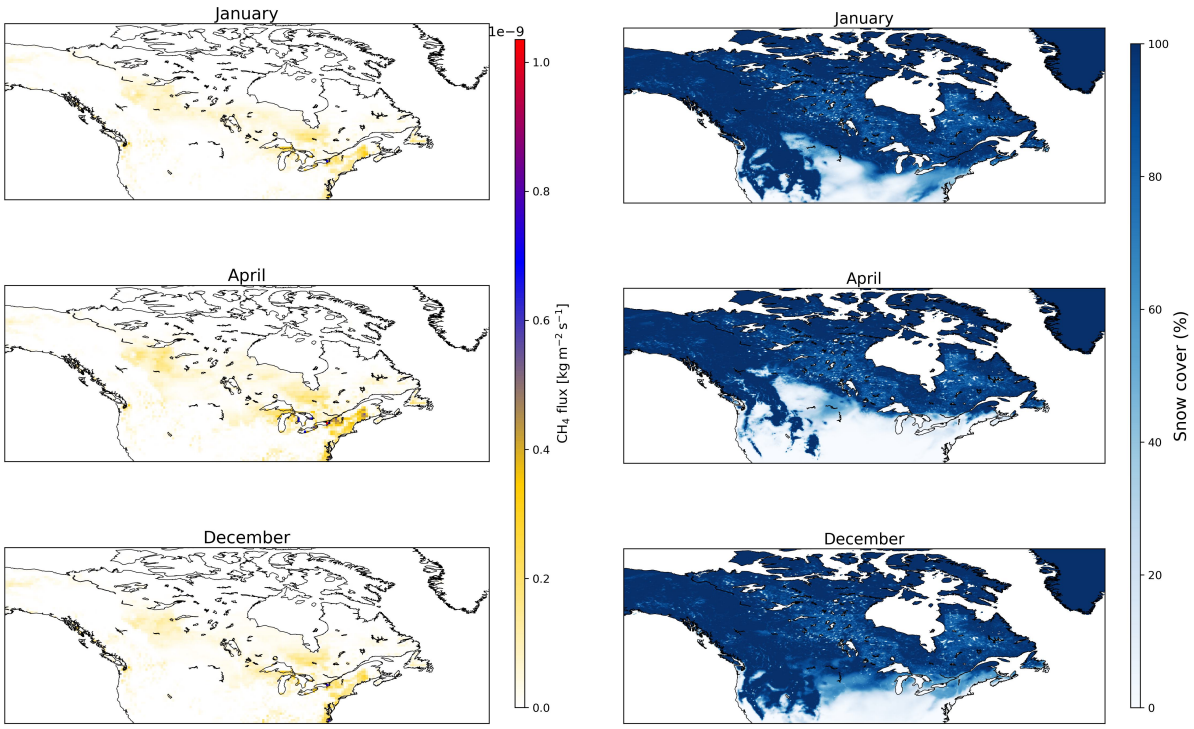

(a) CH_4 flux (b) Snow cover

Figure 3.3.: WetCHART wetland CH_4 fluxes (a) and ERA5-Land snow-cover fraction (b) for January, April, and December 2018 over Canada. Fluxes are shown in kg/m^{2}s and snow-cover as percentage (%) of grid-cell area. Both panels share the same regional bounds (35°–75° N, –150° to –40° E).

The highest CH_4 emissions in Canada, in figure 3.3, can be seen along the shores of the Lakes Superior, Huron and Erie in the south-east of Canada, mainly stemming from peatland complexes and littoral marshes around these lakes [19]. Moreover, spots with higher emission values can be found in the western boreal plains of Canada, which are dominated by bogs and fens [10].

In January and December, nearly all of the Canadian western and central boreal regions lie under a deep snowpack, with the exception of most southerly regions of Canada. In April (fig. 3.3(b)), thawing is not limited to the lowest latitudes, instead a broader latitude strip with less snow cover appears. Additionally, a clear thawing can be seen in regions in mid-latitude central Canada, while areas to the north remain snow-covered.

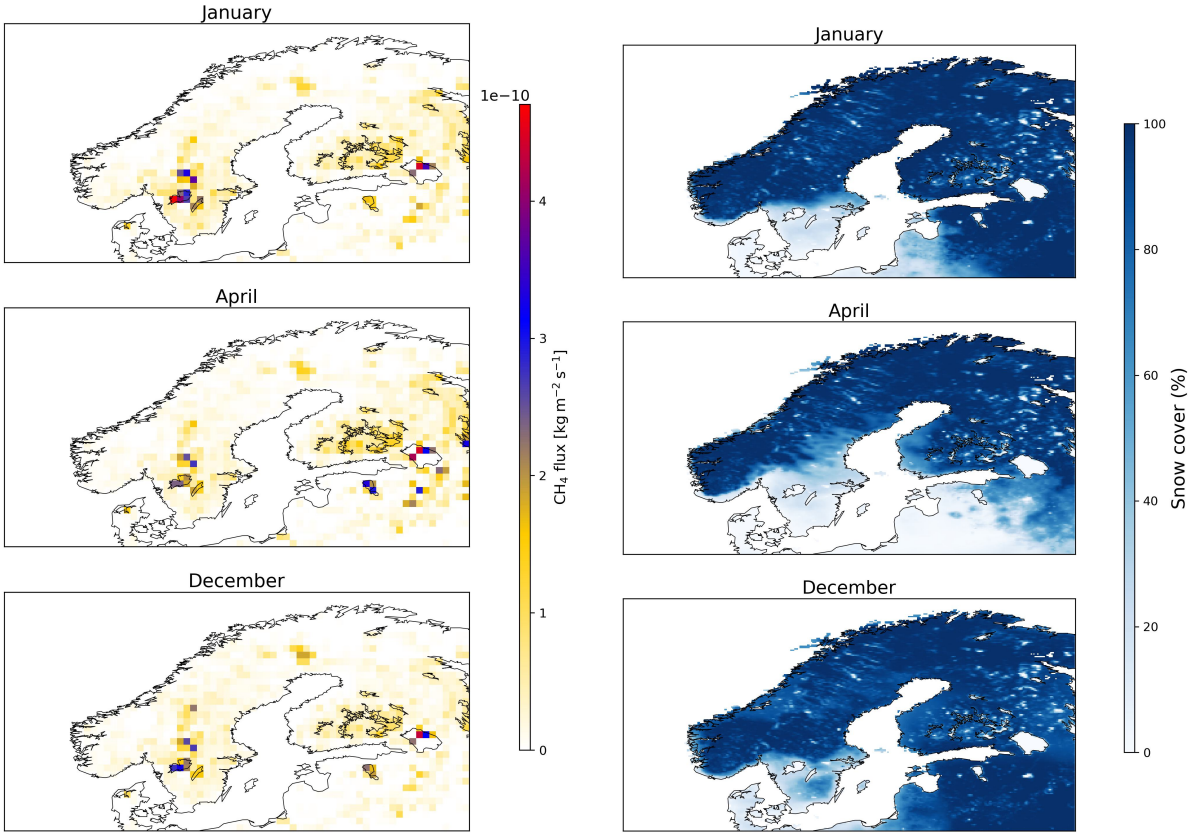

(a) CH_4 flux (b) Snow cover

Figure 3.4.: WetCHART wetland CH_4 fluxes (a) and ERA5-Land snow-cover fraction (b) for January, April, and December 2018 over Scandinavia. Fluxes are shown in kg/m^{2}s and snow-cover as percentage (%) of grid-cell area. Both panels share the same regional bounds (54°–72° N, 0°–35° E).

In Scandinavia (fig. 3.4, the most pronounced CH_4 emission hotspots align with large brackish water bodies, such as Lakes Vänern and Vättern in south-central Sweden or in regions near Lake Ladoga at the Finnish-Russian border. At Lakes Vänern and Vättern, methane is produced by the marsh wetlands that surround the lake margins [17]. In the Lake Ladoga area, methane emissions arise mainly from the shallow peat and marsh wetlands around the shoreline [18]. However, on closer inspection, the emission pixels lie not only around, but also inside all the discussed lakes in the winter months, which should not be possible, because they are completely frozen up during that time. This indicates that there might be inaccuracies in the delineation between wetlands and lakes, or slightly inaccurate mapping of emissions. Moreover, the relatively coarse spatial resolution of the models might be too low to resolve individual lakes. In any case, these hotspots over lakes should be treated with caution. We included figures A.2(a)

and A.2(b), which clearly show these winter lake-hotspots in Scandinavia, in the SI. For Scandinavia, almost the entire landmass is covered in snow in January and December, except for the southern coastal areas in Sweden and Denmark. South-western regions of Finland are under a slightly denser snowpack in January than in December, while the snow covered patches in southern Sweden can only be observed in December, not in January. In April (fig. 3.4(b)), thawing becomes clearly visible as the zone of reduced snow cover pushes farther north into southern Sweden, whereas southwestern Finland, although still snow covered, exhibits substantially thinner and more patchy snow than during the winter months.

Notably, snow depth can also strongly influence CH_4 emissions, because a thinner snow layer might allow gas to diffuse through, whereas a deeper layer can effectively hinder fluxes completely. However, we only wanted to examine, whether a snow-cover effect may explain parts of the winter overestimations in wetCHART overall, without providing a detailed analysis of the dependence on the snow depth.

While the emissions generally coincide with known wetlands and in some areas mirror the snow cover patterns, WetCHART also predicts fluxes across vast regions that remain deeply snow covered throughout all the months, shown in figures 3.3 and 3.4. This indicates that the model does not fully account for snowpack trapping of methane, which explains a part of the overpredictions of wetCHART fluxes during the winter months.

3.2. Analysis of the CAMS mixing ratio data

As a next step, we analyse the CAMS concentration data, described in section 2.1 for the two regions. Initially, we show the wetland fluxes CAMS used as a priori fields for their simulation. This allows us to compare them with the resulting concentrations, which are calculated from all sources, not only wetlands [4]. The wetland emissions are depicted as an average over summer (May-Aug) and winter months (Nov-Feb), with a capped colour bar at 1e-9 kg/m^{2}s, to visualize fluxes from mid to low emission areas.

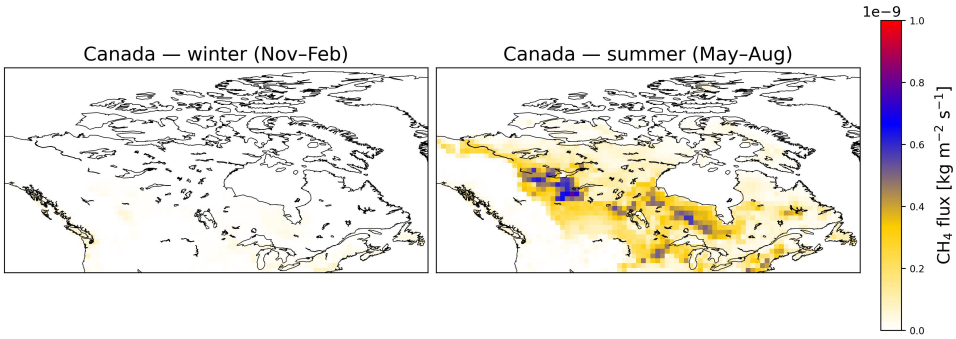

(a)

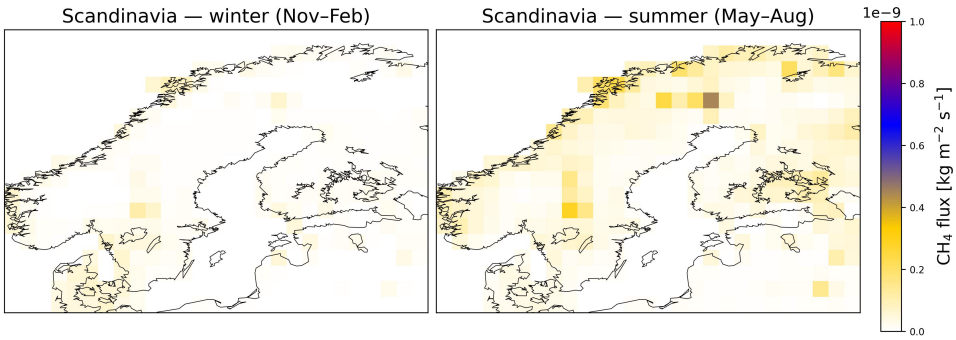

(b)

Figure 3.5.: Seasonal mean wetland CH_4 fluxes by CAMS (2018) in kg/m^{2}s, shown for winter (Nov-Feb, left) and summer (May–Aug, right) months over Canada (a) and Scandinavia (b). The colour scale is capped at 1e-9 kg/m^{2}s.

As depicted in figure 3.5, the wetland CH_4 fluxes exhibit a strong seasonality for both regions. While emissions remain sparse and low during winter, the increased release of methane from wetlands in warmer months (see section 1.3.2) leads to an increase of fluxes over wetland areas during the summer. This is in alignment with the overall seasonal patterns described in section 3.1.1.

The concentrations in the datafiles include hybrid sigma pressure coordinates. To make the model levels visually comparable with other datasets with altitude layers only, we estimated the geometric height of each model level by globally averaging the altitude values of the two surrounding half-levels for figures 3.6 and 3.7.

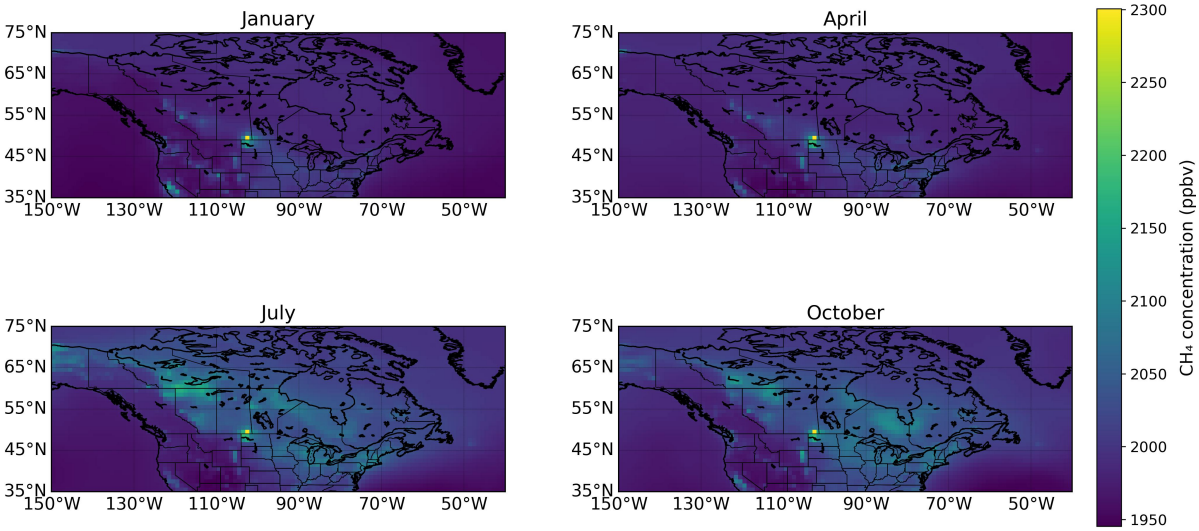

Figure 3.6.: Monthly averaged CAMS methane concentrations in ppbv for an averaged altitude of $\sim$ 410 m in Canada, for January, April, July and October 2022. The concentrations are shown for the regional bounds: 35° to 75° N and –150° to –40° E.

Figure 3.6 depicts methane concentrations over Canada for four different months, to allow for a closer examination of the seasonality. The figures clearly illustrate a seasonal pattern, where increasing emissions towards the warmer months result in higher methane concentrations in the atmosphere. The concentrations then decrease towards the colder months in winter, mirroring the wetland flux patterns in figure 3.5(a). This already suggests that wetlands alone describe a large part of the emission landscape during the summer months when they are most active. We further explore this hypothesis during the course of this chapter.

Furthermore, three regions with high emissions are especially noticeable, where emissions do not follow any seasonality. Firstly, there is a hotspot in the south east of Saskatchewan at the border to the USA and Manitoba, within the Williston Basin, which contains many gas and oil fields, such as "Sinclair", "Fertile" and "Three Forks". Secondly, a spot in central Alberta near the border to British Columbia lies in the Montney "tight gas" region. Lastly, an area in the north east of British Columbia, close to Alberta, corresponds to condensate-rich sections of the Montney Formation around the Kakwa River sour-gas processing plant [14].

We investigated the anthropogenic input flux fields used by CAMS and confirmed that all the regions discussed above are clearly represented. To illustrate this, we have added figure A.1(a) to the Supporting Information (SI).

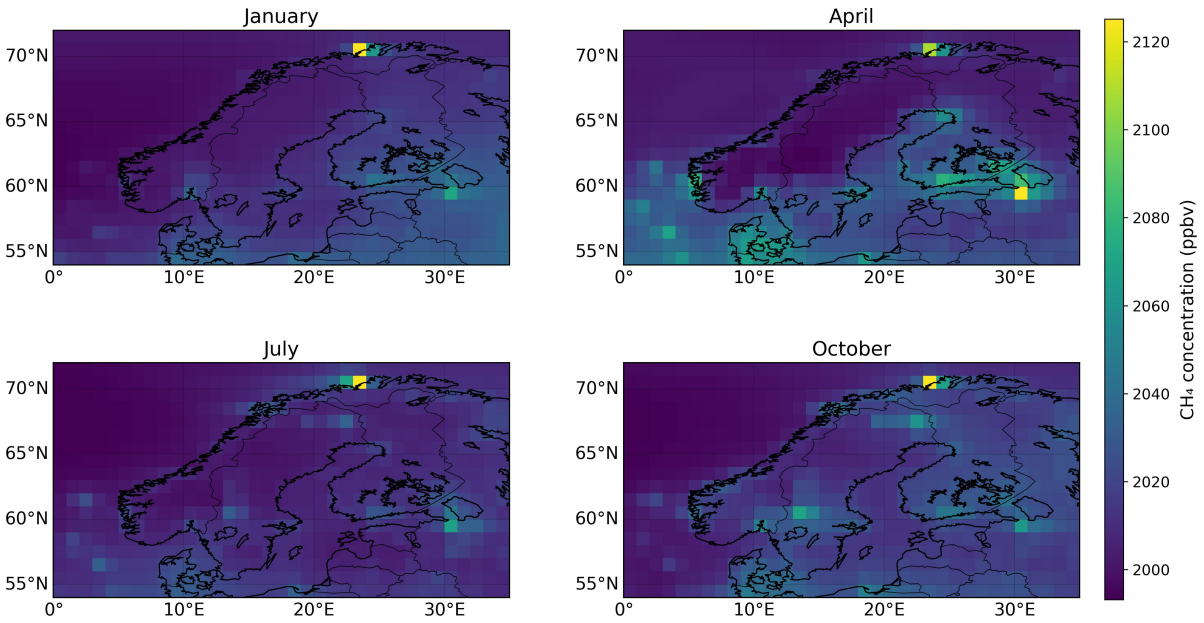

Figure 3.7.: Monthly averaged CAMS methane concentrations in ppbv for an averaged altitude of $\sim$ 410 m in Scandinavia, for January, April, July and October. The mixing ratios are depicted for a latitude/longitude area of 54°–72° N and 0°–35° E.

Figure 3.7 shows the seasonal CH_4 concentrations over Scandinavia. In contrast to the Canadian concentrations, the distinct seasonal patterns in the wetland fluxes, illustrated in figure 3.5(b), are not mirrored in the resulting concentrations in Scandinavia. The seasonality of the wetland fluxes can only clearly be observed in the concentrations for the wetlands in the Sjaunja mire system in northern Sweden and for wetlands north of Lake Vänern. Here, the wetland emissions remain elevated well into autumn, indicating a longer active season compared to Canada. Furthermore, figure 3.7 clearly depicts high mixing ratios around Lake Ladoga throughout the year, which can also be seen in the fluxes of figure 3.5(b). However, the lack of clear, distinct seasonality in this case and overall suggests that, besides wetlands, anthropogenic emissions might play a crucial role here. Therefore, we also examined the anthropogenic input fluxes by CAMS for Scandinavia, as shown in figure A.1(b) in the SI. From this analysis we concluded that the peak around Lake Ladoga is actually more likely linked to discharges from pulp and paper operations and adjacent wastewater outlets along the shores of Lake Ladoga [12], as we could see high emissions in this area year round. The most distinct hotspot at around 70°N is also found in the anthropogenic fluxes and most likely stems from offshore Liquid Natural Gas (LNG) and oil and gas fields in the Barents Sea [13]. Although, boreal wetlands emissions play an important role in Scandinavia, as depicted

in figure 3.5(b), the simulated concentrations by CAMS seem to be driven more by anthropogenic fluxes [4, 35] in this region. Thus, we conducted further examinations on this assumption.

3.3. Bias analysis: Canada

As an initial step, before we compared the CAMS concentrations to measurement data from the NOAA Obspack data package from section 2.2, we conducted Source Receptor Relationship (SRR) simulations for individual stations (see section 2.3) to assess their respective area of influence. We computed daily sensitivities or "Footprints" in the unit of m^3s/kg and later averaged them over our summer (May-Aug) and winter months (Nov-Feb).

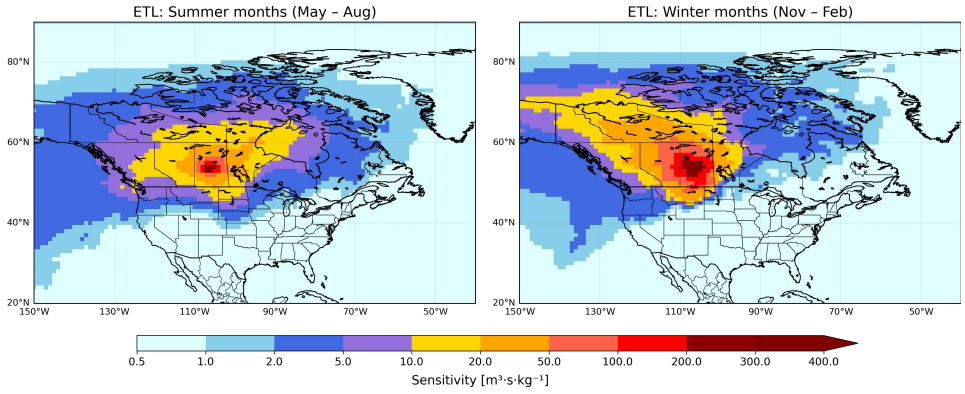

(a)

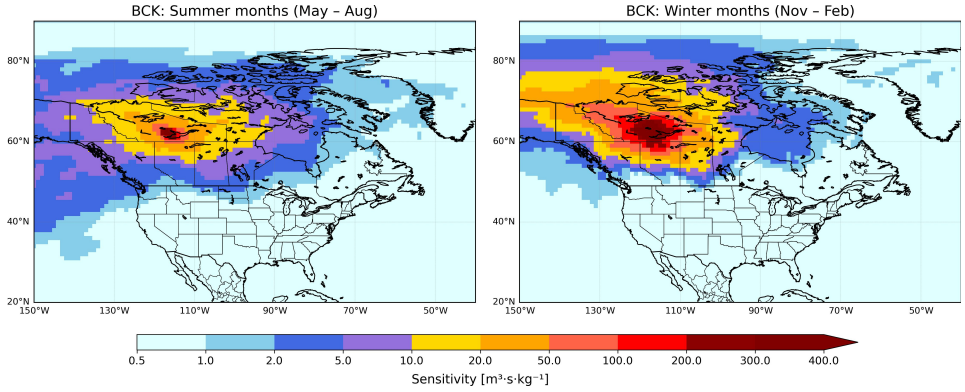

(b)

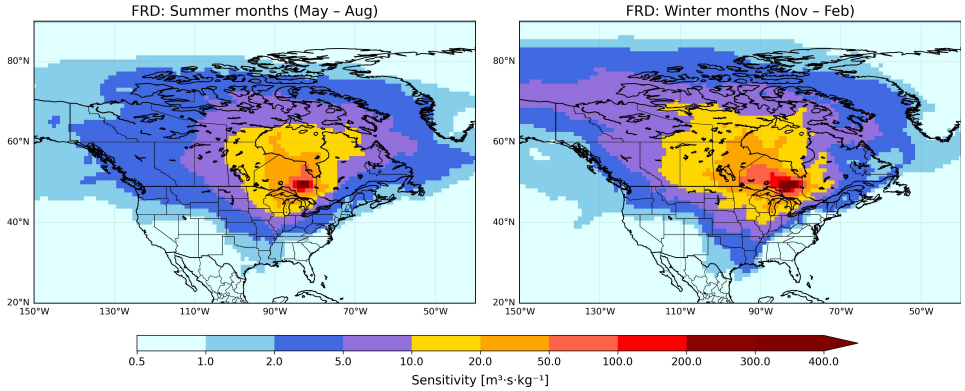

(c)

Figure 3.8.: The footprints in m^3s/kg averaged over summer (May-Aug) and winter months (Nov-Feb) for the measurement stations East Trout Lake (ETL, a), Behchoko (BCK, b) and Fraserdale (FRD, c) in Canada.

For ETL (Fig. 3.8(a)), winter sensitivities reach high values across a broad area of influence around the station, extending northwestwards across Canada. For the summer months this area of influence shrinks significantly to a much more localized area with

peak values above the wetlands surrounding the ETL station. The same pattern can be seen for the BCK station in figure 3.8(b), while this seasonal effect is a lot less pronounced for FRD in figure 3.8(c). The overall westward extension of the footprint-areas during winter can be explained by the faster atmospheric circulation (westerly winds), compared to the more stagnant summer circulation.

To quantify each station's CH_4 mixing ratio response, we multiplied the daily footprint sensitivities at each grid cell by the four wetland scenario fluxes discussed in this work, as well as the anthropogenic emission prior fluxes by CAMS and then converted those products into volume mixing ratios in the unit of ppbv, using the procedure, described by Seibert et al., (2004) [37]. Summing over all grid cells yields the net contribution from each source category at the respective measurement site, accumulated over the duration of the transport simulation. Figure 3.9 shows the monthly mean contributions (ppbv) at ETL, BCK and FRD for 2022. Notice that "background" concentrations of methane, not accounted for during the period of the backward simulations, would have to be added to explain the measured concentrations. However, the background signal is determined by the global distribution of sources.

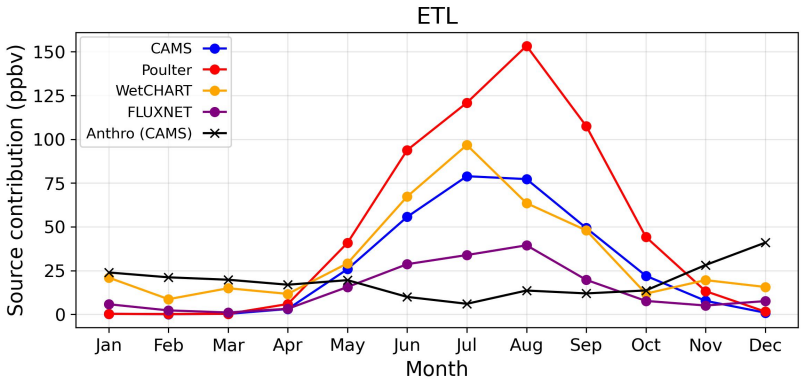

(a)

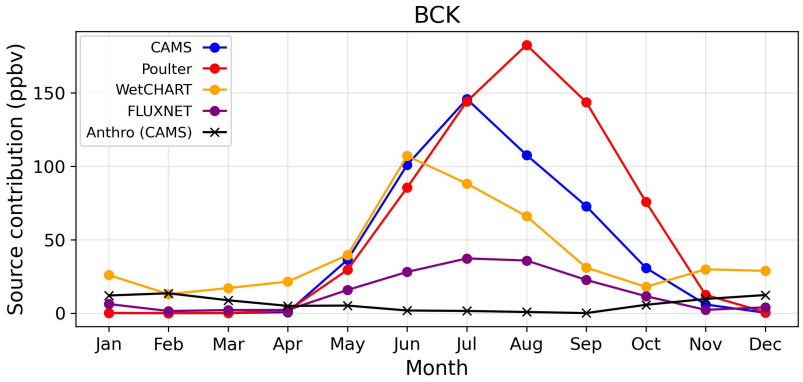

(b)

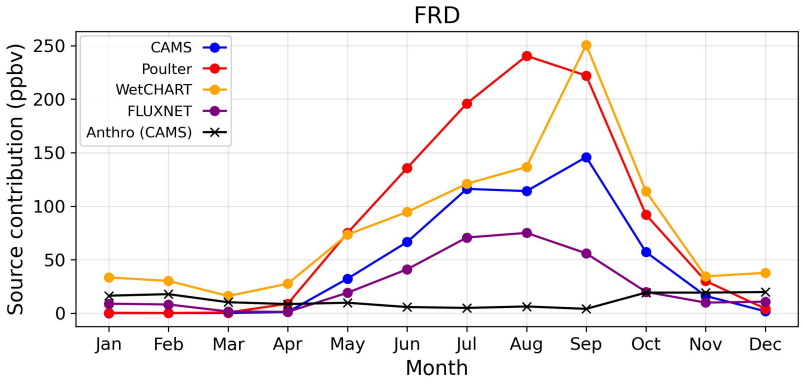

(c)

Figure 3.9.: Monthly mean CH_4 source contributions in ppbv, accumulated over 15 days via a FLEXPART SRR simulation, at the Canadian stations ETL (a), BCK (b) and FRD (c) in 2022. The wetland contributions are depicted for the wetland scenarios: wetCHART (orange), FLUXNET (purple), Poulter et al. (2017) (red) and CAMS (blue). The depicted anthropogenic contributions by CAMS (black) serve as a reference for the relative magnitude of wetland versus anthropogenic sources.

The vast majority of emissions in Canada come from wetlands, followed by anthropogenic sources. Wetlands emit around $\sim$ 20 Tg per year, which is roughly 5 times as much as all combined anthropogenic releases ($\sim$ 4 Tg per year) [3]. It can clearly be seen in figure 3.9, that wetlands dominate the measured concentrations at all three stations, which is consistent with what has been reported previously [3]. All the stations show the expected seasonal patterns for both wetland and anthropogenic contributions. Wetland contributions are near zero in winter and increase during spring to a maximum in mid-summer, before they decrease again towards the winter. In contrast, anthropogenic sources contribute relatively steadily throughout the year, with only modest increase during late autumn and winter. Possible explanations for this increase are actually higher emissions (e.g. increased fossil fuel use for heating), or the reduced vertical mixing in colder months, which traps methane closer to the surface, thereby increasing surface emissions. Investigating the relative importance of these factors would be a valuable avenue for future research.

For all the three sites, the FLEXPART-derived wetland contributions from Poulter et al. (2017) consistently estimate the highest contributions throughout the year, while FLUXNET shows the lowest contributions out of the 4 models. CAMS and wetCHART fall between these extremes, except for a large wetCHART peak at FRD in September. As discussed in Section 3.1.2, parts of the higher winter estimates by wetCHART, are explained by inaccuracies in modelling snowpack trapping effects.

Furthermore, figure 3.9 shows that from the three stations, ETL is influenced most by anthropogenic emissions. However, due to the very sparse temporal measurement density at FRD, we chose to examine the model bias for the wetland driven stations BCK and ETL for Canada.

Of course, the CAMS concentration fields use methane input fluxes from various natural and anthropogenic sources, not just wetlands. To isolate the wetland signal, we therefore subtract the monthly median mixing ratios at the “background” station Alert (ALT) from both the modelled and observed concentrations at our wetland-driven sites, to reveal the ”enhancements” at these stations. Since anthropogenic sources typically exhibit only modest seasonal variation and wetlands dominate the signal, we expect any observed seasonality of the corrected biases to predominantly reflect wetland seasonality. The ALT station in the north east of Ellesmere Island in Nunavut is well suited as a background station, as it is snow covered for about ten months of the year and is spatially seperated from major methane emission sources [43]. Background correction carries inherent limitations: CH_4 for example has a pronounced, seasonally varying latitudinal

gradient, so using a high-Arctic site like Alert can leave residual latitude-dependent biases at boreal stations. Nonetheless, ALT proved to be a good compromise for our study and has been employed successfully in other research [43].

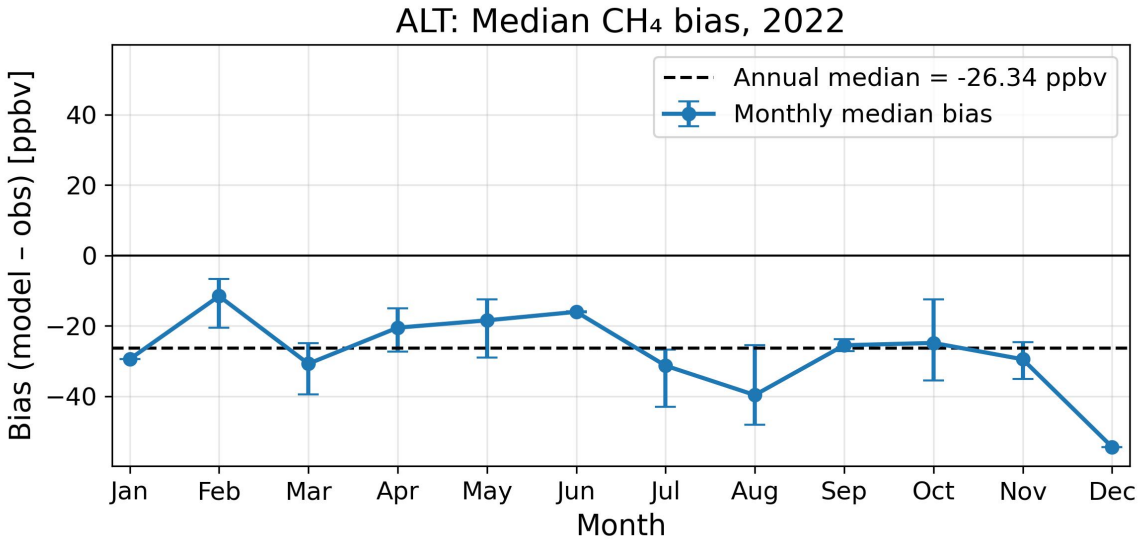

Figure 3.10.: Monthly averaged median model–observation CH_4 bias for the CAMS model at the Alert (ALT) background station for 2022. Markers show the monthly medians, the dashed line indicates the annual median bias (–26.34 ppbv), and the vertical bars span the interquartile range (25th–75th percentile).

Figure 3.10 shows that at ALT the CAMS model consistently underestimates observed CH_4 throughout 2022. The monthly averaged median bias ranges between approximately –10 ppbv (February) and –55 ppbv (December), with an annual median of –26.34 ppbv. No error bars are shown for January, June and December, because there was only one measurement available in these months. To further explore this consistent negative bias, we checked the collective median bias over all stations within a latitude range between 50 to 70°N and -140 to -50°E. This was done to enquire, whether this negative bias is unique to ALT or part of a broader regional pattern across multiple stations, covering wetland rich areas in Canada as well as the area around ALT. A selection of this area was made to include as many high-emitting wetlands as possible while excluding areas heavily influenced by other sources and this area proved to be a suitable compromise.

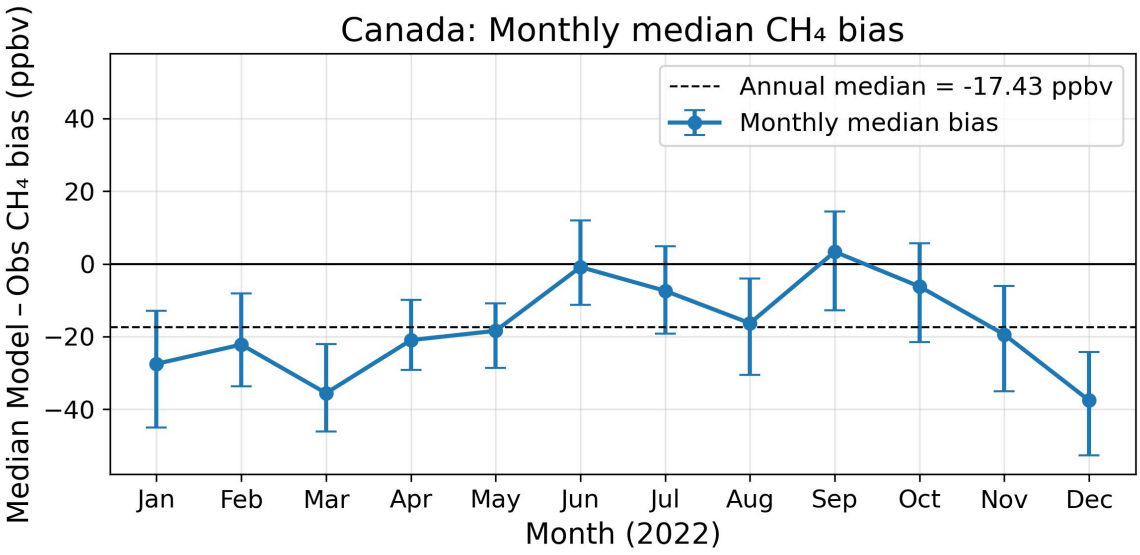

Figure 3.11.: Monthly median model–observation CH_4 bias for all stations in the 50–70° N, –140 to –50° E region during 2022. Markers show the monthly medians, the dashed line indicates the annual median bias (–26.34 ppbv), and the vertical bars span the interquartile range (25th–75th percentile)

Figure 3.11 presents the monthly median model–observation CH_4 bias aggregated over all NOAA stations within the 50–70° N, –140 to –50° E area for 2022. Biases range from a minimum of –38 ppbv in December to a maximum of +3 ppbv in September. During summer months (June–September), the median bias is relatively close to zero, while the winter months (November-February) exhibit large negative biases. This shows that CAMS possibly either underestimates CH_4 emissions or overestimates OH removal, throughout the year, but especially during colder winter months and that the under-prediction is not unique to the ALT station, but part of a broader, regional pattern. Apart from the possible underestimation for CH_4 emissions, another explanation could be related to the applied OH concentrations. The production of OH radicals in the atmosphere requires UV sunlight (see section 1.3.2), which is why the OH levels drop during the darker high latitude winter months. Hence, a possible explanation for a part of this latitude dependent underestimation of emissions is that the CAMS model does not fully capture the seasonal decline in OH radical concentrations at high latitudes during winter, leading to an overestimation of CH_4 sink during these darker months [24].

Subsequently, we computed the background-corrected median biases at ETL and BCK by initially subtracting the monthly median concentration at the background station

(ALT) from both the modelled and observed values (Fig. 3.12).

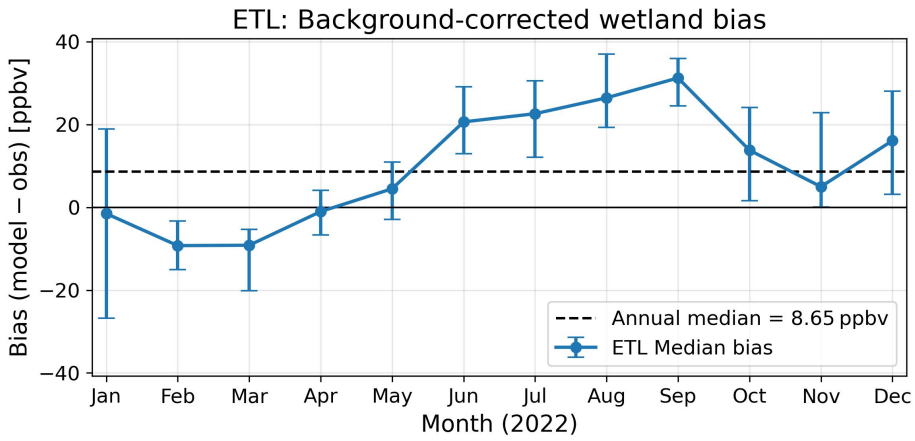

(a)

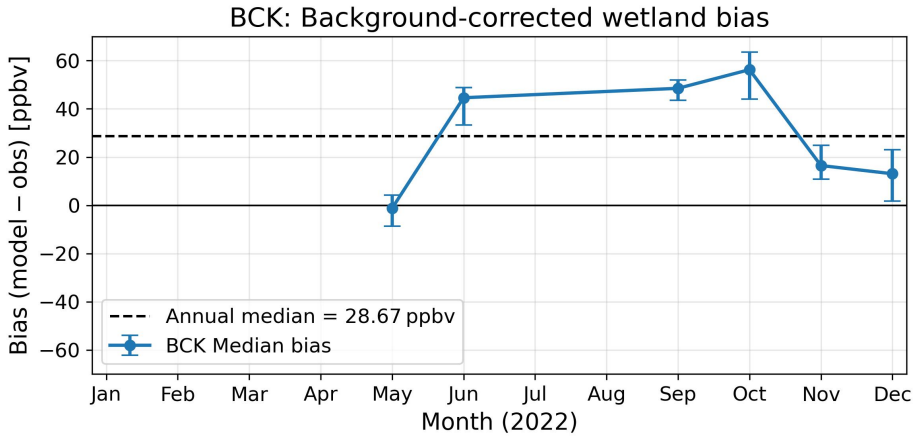

(b)

Figure 3.12.: Monthly median model–observation bias after subtracting the monthly averaged mixing ratios of the background station (ALT) from the observations and CAMS model concentrations at East Trout Lake (ETL, a) and Behchoko (BCK, b) for 2022. Markers show the background-corrected monthly medians, the dashed line indicates the annual median bias (ETL: +8.7 ppbv, BCK: +28.7 ppbv) and the error bars span the interquartile range (25th –75th percentile).

At ETL (Fig. 3.12(a)), the background-corrected bias remains slightly negative through early spring, with minima just above $\sim$ –10 ppbv in February and March, before climbing steadily to a late summer peak of $\sim$ +30 ppbv in September. After September, the bias decreases again, with an annual median of +8.65 ppbv.

For BCK (Fig. 3.12(b)), the wetland bias is near zero in May, then jumps to +45 ppbv in June and rises further to +56 ppbv in October. It drops sharply to +16 ppbv in November and +13 ppbv in December, yielding an annual median of +28.67 ppbv. There are no observations from January to April and again from July to August, but it is unlikely that filling those gaps would change the clear seasonal overprediction seen in the warmer months (June and September), because the measured months already include the start and end of peak wetland emissions and methane fluxes typically only change gradually over the summer. Similarly, because wetland emissions are essentially zero in winter, we do not expect the bias to flip above zero during the missing January–April period. This is also backed by figure 3.9, which shows that the wetland influence on BCK follows the seasonality, typical for wetlands. The results from this analysis indicate that CAMS consistently overestimates wetland emissions, particularly during the summer months when wetlands are the dominant CH_4 source.

As previously discussed, the wetland emissions for different wetland scenario models exhibit a large variability. Therefore, a potential avenue for future research could be to use a wetland emission scenario with lower estimates than CAMS during the summer months in order to reduce the positive wetland bias during that time in Canada. To test which of the examined wetland scenarios in this thesis produces the lowest biases for ETL and BCK, we calculated the FLEXPART source contributions in ppbv for wetCHART, FLUXNET and Poulter et al. (2017), just like we did for CAMS in figure 3.9. Subsequently, we calculated the differences of the monthly means between CAMS and the other three models and added these values to the background-corrected median biases of figure 3.12. This effectively replaces the CAMS-derived wetland contribution with the FLEXPART-computed contributions from each alternative scenario, approximating the bias that would result from using the other wetland scenario models as prior fluxes for the CAMS inversion.

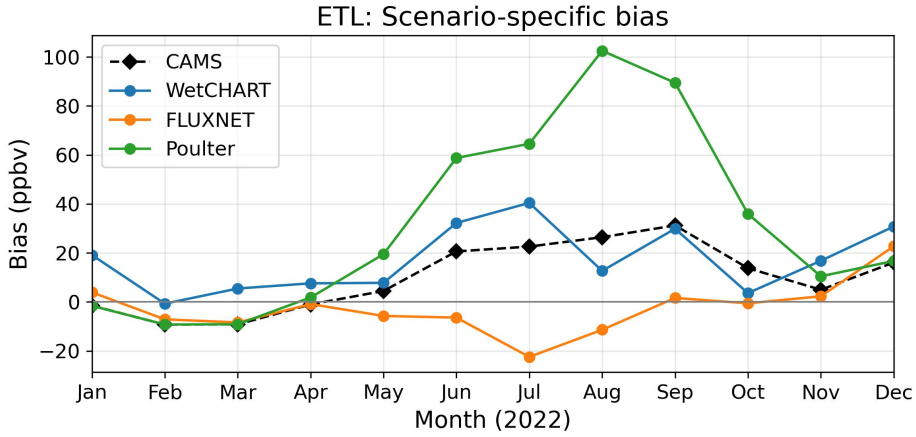

(a)

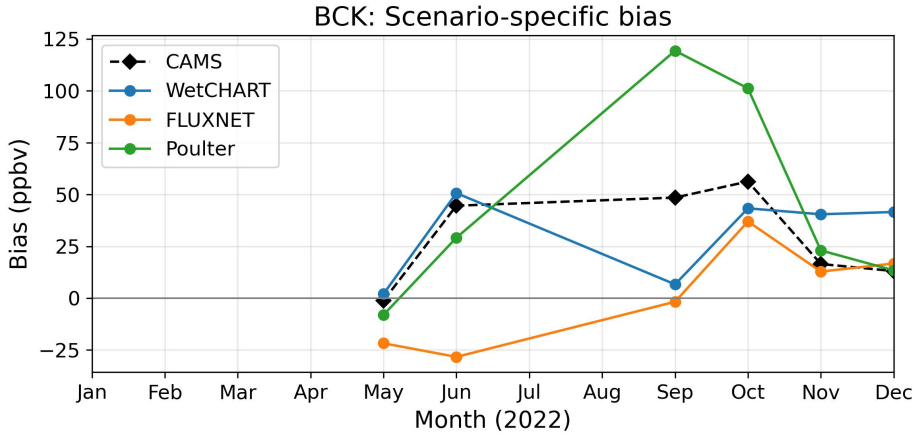

(b)

Figure 3.13.: Monthly background-corrected model–observation CH_4 median biases at (a) East Trout Lake (ETL) and (b) Behchoko (BCK) for 2022. The dashed black lines show the CAMS reference bias, while the coloured lines show the scenario-specific biases for wetCHART, FLUXNET and Poulter et al. (2017), obtained by adding each monthly (scenario – CAMS) difference to the CAMS median bias.

Figure 3.13 shows that for both stations, Poulter et al. (2017) would further enhance CAMS's summer overpredictions, while wetCHART produces biases similar to CAMS during the active season, yet overpredicts throughout winter, which was previously described in section 3.1.2. In contrast, FLUXNET exhibits negative biases during summer, but otherwise remains close to CAMS. Despite, FLUXNET showing negative summer biases, thereby likely underestimating summer emissions, the annual median bias is lower

than for CAMS at both stations (–3.31 ppbv for ETL and 5.55 ppbv for BCK). From this analysis, we conclude that both wetCHART and FLUXNET emerge as potentially promising emission priors, when computing concentration fields over Canada. However, the winter overpredictions by wetCHART, which are an artefact of insufficiently modelling snow-covered methane trapping, should be corrected by applying a suitable snow cover mask (e.g. ERA5-Land reanalysis [27]). As can clearly be seen in figure 3.13, the Poulter et al. (2017) ensemble produces substantially larger positive summer biases than the other three scenarios and is therefore unlikely to serve as a suitable wetland flux prior for Canada.

Notably, we only analysed two wetland-dominated stations in Canada, so these findings might not be representative of all such sites. As an avenue for future research, we suggest applying this methodology to an ensemble of wetland-dominated stations throughout Canada, instead of individual stations. By testing an ensemble of wetland-dominated stations, we can identify which priors consistently minimize biases across different environments. Reducing overall wetland model biases is of great importance for improving the ability to fully grasp the global wetland methane budget with more accurate models, as emphasized in the Introduction (sec. 1).

3.4. Bias analysis Scandinavia

We also applied the same bias analysis, discussed in section 3.3, for the Scandinavian region. Firstly, we computed the average footprints over summer (May-Aug) and winter (Nov-Feb) for the stations PAL, SVB and PUI, which are described in section 2.3.

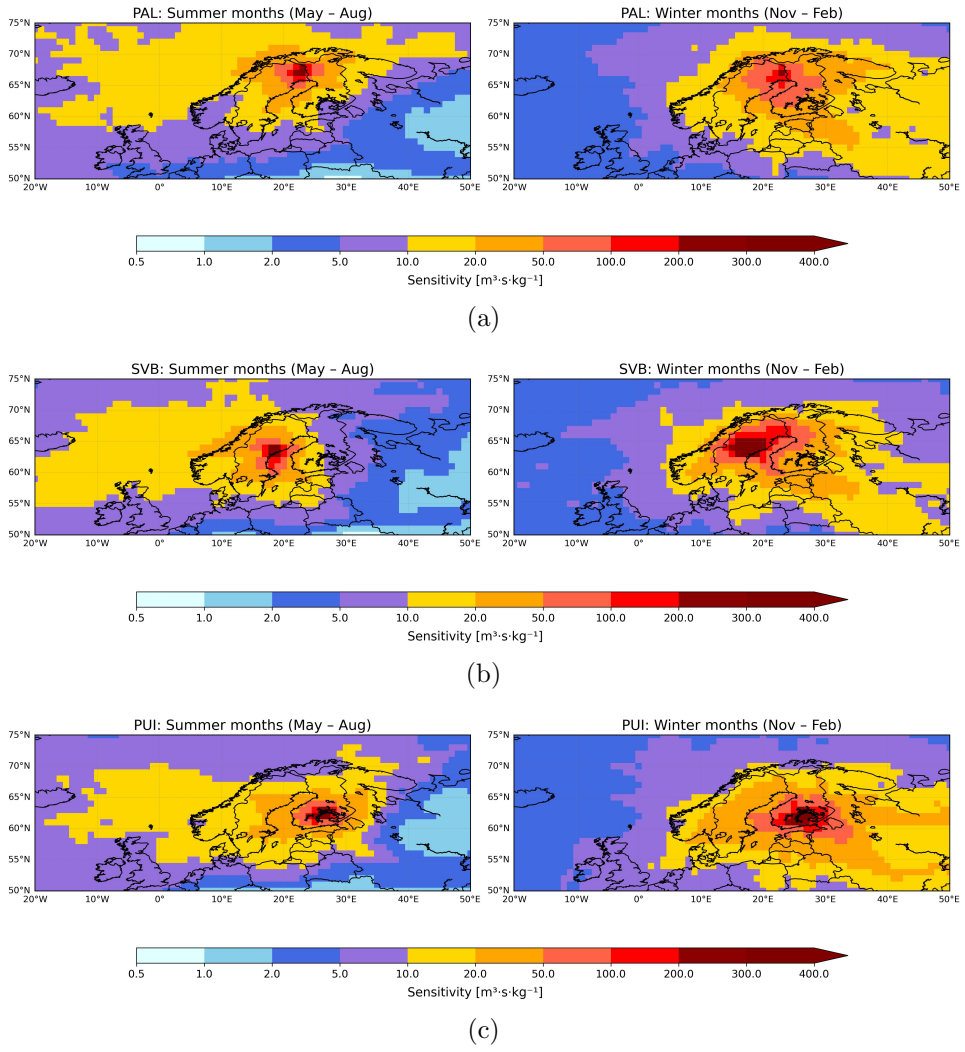

Figure 3.14.: The footprints in m^3s/kg averaged over summer (May-Aug) and winter months (Nov-Feb) for the measurement stations Pallas (PAL, a), Svartberg (SVB, b) and Puijo (PUI, c) in Scandinavia.

For PAL (fig. 3.14(a)), winter footprints maxima near the station (right panel) are relatively low and broadly distributed across Scandinavia, with influences from the Barents Sea and Russia. In summer (left panel), the high-sensitivity area peaks over the Sjaunja mire complex area immediately surrounding the PAL station. Furthermore, it can be seen that PAL also measures a substantial fraction of emissions that were advected across the European Arctic Ocean and the Barents Sea into Scandinavia. The same pattern can be observed for SVB (fig. 3.14(b)), where the highest sensitivity areas in winter are broadly spread across Scandinavia, including influences from Russia and the Barents Sea. During summer, the sensitivity peaks over the wetlands around the SVB

station. The increase in influence from the Barents sea and the European Arctic Ocean, compared to the winter, can also be seen for SVB. While PUI (fig. 3.14(c)) also shows the same described influences as the other two stations, its sensitivity remains slightly more broadly distributed throughout the year, with less localized hotspots, around the wetlands near PUI station during summer.

In the same way as for the Canadian stations ETL and BCK, we calculated the contributions of wetland and anthropogenic emissions on the measured concentrations of the Scandinavian stations PAL and SVB in 2022. The monthly averages of these contributions are depicted in figure 3.15.

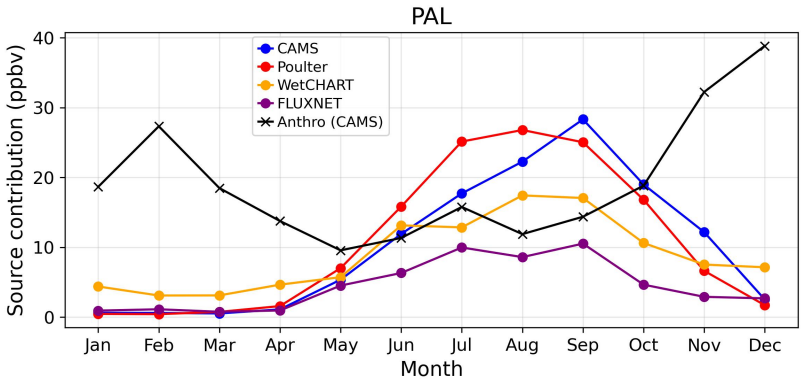

(a)

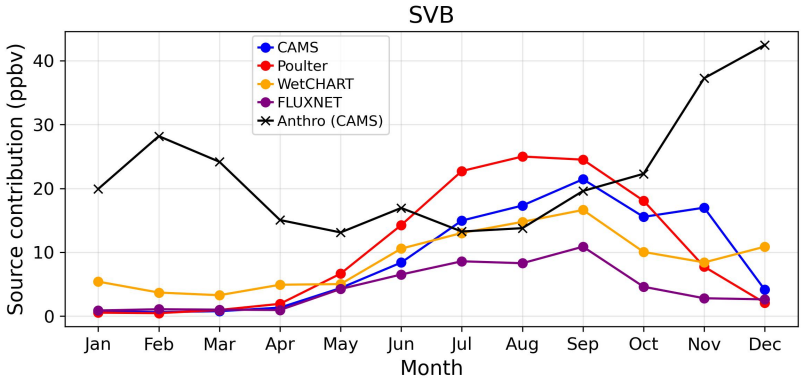

(b)

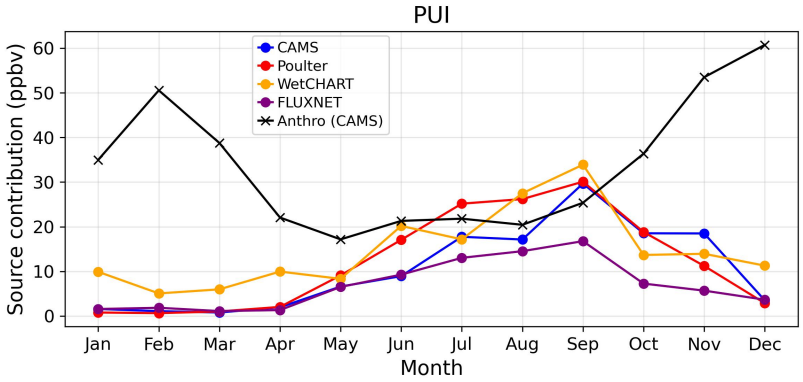

(c)

Figure 3.15.: Monthly mean CH_4 concentration contributions in ppbv at the Scandinavian stations PAL (a), SVB (b) and PUI (c) in 2022. The wetland contributions are depicted for the wetland scenarios: wetCHART (orange), FLUXNET (purple), Poulter et al. (2017) (red) and CAMS (blue). The depicted anthropogenic contributions by CAMS (black) serve as a reference for the relative magnitude of wetland versus anthropogenic sources.

Once again, the typical seasonal wetland pattern is evident in figure 3.15: influence rises during the warmer months and then declines through autumn and into winter. Compared to the Canadian patterns, the decline in autumn emissions here is more gradual and continuous through the autumn and winter months for all stations.

At both PAL and SVB, the Poulter et al. (2017) scenario produces the highest wetland contributions for most of the year and FLUXNET the lowest throughout the year, with CAMS and wetCHART falling in between. However, at PAL, CAMS slightly exceeds Poulter et al. (2017) from September to December, whereas at SVB this is the case in November and December. While this ranking mirrors the pattern seen at the Canadian stations (see fig. 3.9) for PAL and SVB, the overall spread between the four scenarios is notably smaller. At PUI, the differences between the models are even smaller, compared to the other two stations. Here, FLUXNET remains the lowest year-round, while wetCHART and Poulter et al. (2017) show the highest, closely matching contributions and CAMS lies just below them. The anthropogenic influences show an increase during the winter months in all panels, with maxima in December($\sim$ 40 ppbv for PAL and SVB and $\sim$ 60 ppbv at PUI) and a local maximum in February ($\sim$ 30 ppbv at Pal and SVB and $\sim$ 50 ppbv for PUI). The anthropogenic summer contributions range from approximately 10-20 ppbv, with the highest values at PUI. As described in section 3.3, this increase in anthropogenic winter contributions likely either shows actually higher emissions, or is a result of reduced vertical mixing in colder months. It can clearly be seen from figure 3.15, that FLUXNET's wetland contribution stays below the anthropogenic contribution at all three sites. During the peak-emission months from July to September, the Poulter et al. (2017) scenario surpasses anthropogenic emissions by more than 10 ppbv at PAL, by a smaller margin at SVB and only slightly at PUI. During these peak-emission motnhs, the CAMS wetland contributions also exceed the anthropogenic contributions substantially at PAL, only slightly at SVB, yet remain below the anthropogenic line throughout the year, except for September. The wetCHART contributions exceed the anthropogenic ones slightly in August and September at PAL and PUI, but fall below the anthropogenic curve otherwise. At SVB, wetCHART contributions likewise remain below the anthropogenic curve throughout the year, while matching them closely in July and August. Unlike in Canada, where wetlands overwhelmingly dominate the summer budget, multiple sources in Finland (PAL and PUI) and Sweden (SVB), such as livestock and waste, oil and gas production, or geological sources, contribute at more comparable magnitudes throughout the year [8, 29, 39], which is clearly reflected in our results from the source contribution analysis (fig. 3.15).

Among all sites, PUI shows the highest anthropogenic-to-wetland CH_4 contribution ratio, while PAL exhibits the lowest. Consequently, as this thesis focusses on the wetland emissions, we will use the stations PAL and SVB for our comparison with measurement data. Thereafter, just like in section 3.3, we again subtracted a background from the modelled, as well as observed mixing ratios. For Scandinavia, we used the Mace Head (MHD) station as a background. The MHD station is located on the west coast of Ireland, is largely isolated from continental emissions and provides a regionally relevant background for the analysis of Scandinavian stations [16]. Notably, no observations were available for MHD in September or October, so we used the monthly averaged August mixing ratio for September and the November average for October when subtracting the background from both modelled and observed values. At a remote background site, month to month variations are typically small. Therefore, this substitution should not affect the overall patterns of the calculated biases. In Scandinavia, both anthropogenic and wetland CH_4 emission inventories carry substantial uncertainties. The combination of similarly high emission sectors and large dataset uncertainties, together with our findings in figure 3.15, makes it difficult to isolate a single dominant source. As a result, we do not expect to see any clear seasonal wetland bias pattern for Scandinavia. However, by subtracting the background concentrations, we hope to remove a large fraction of the advected CH_4 signal (see fig. 3.14), so that the the remaining signal more closely reflects regional emissions around the PAL and SVB stations.

From here, we followed the same methodology used for Canada. Initially, we again computed the median biases for the background station MHD in figure 3.16.

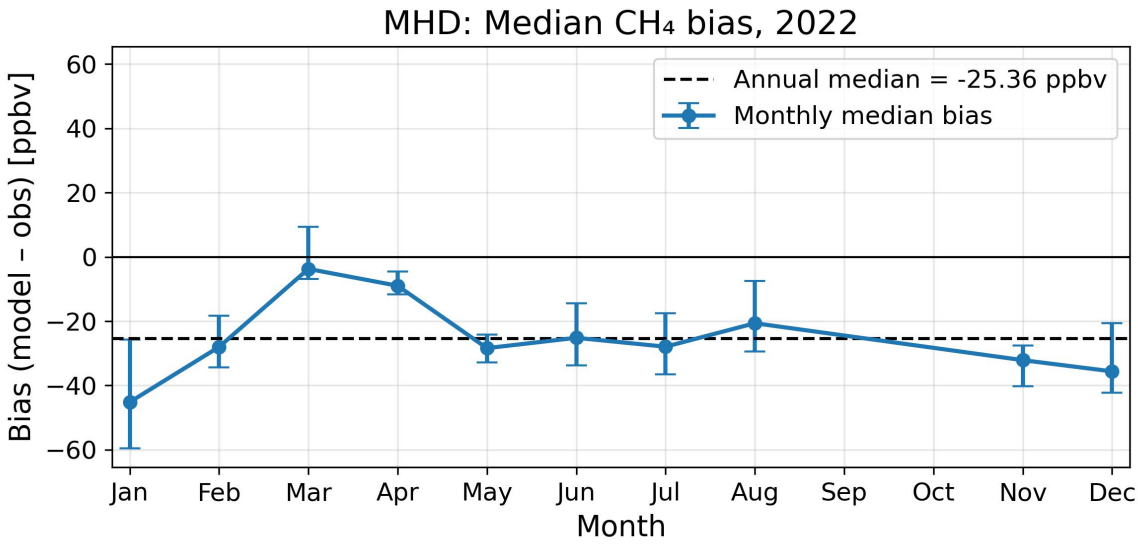

Figure 3.16.: Monthly averaged median model–observation CH_4 bias at the Mace Head (MHD) background station for 2022. Markers show the monthly medians, the dashed line indicates the annual median bias (–25.36 ppbv), and the vertical bars span the interquartile range (25th–75th percentile).

Figure 3.16 shows that at Mace Head (MHD) the CAMS model biases are negative throughout the year, with biases spanning from a minimum of –45 ppbv in January to a maximum of –5 ppbv in March and an annual median bias of –25.36 ppbv. Overall, the negative biases are the most pronounced during the colder winter months December and January. The model emissions are slightly closer to the measured mixing ratios between May and August ($\sim$ -22 ppbv bias) and the bias is within 5 ppbv in March and April.

Furthermore we checked for a potential regional and seasonal bias pattern, by calculating the aggregated bias over all stations within a latitude range of 56 to 70 °N and -10 to 34° E, covering the entire wetland landscape over Scandinavia, while keeping influences from surrounding regions as low as possible.

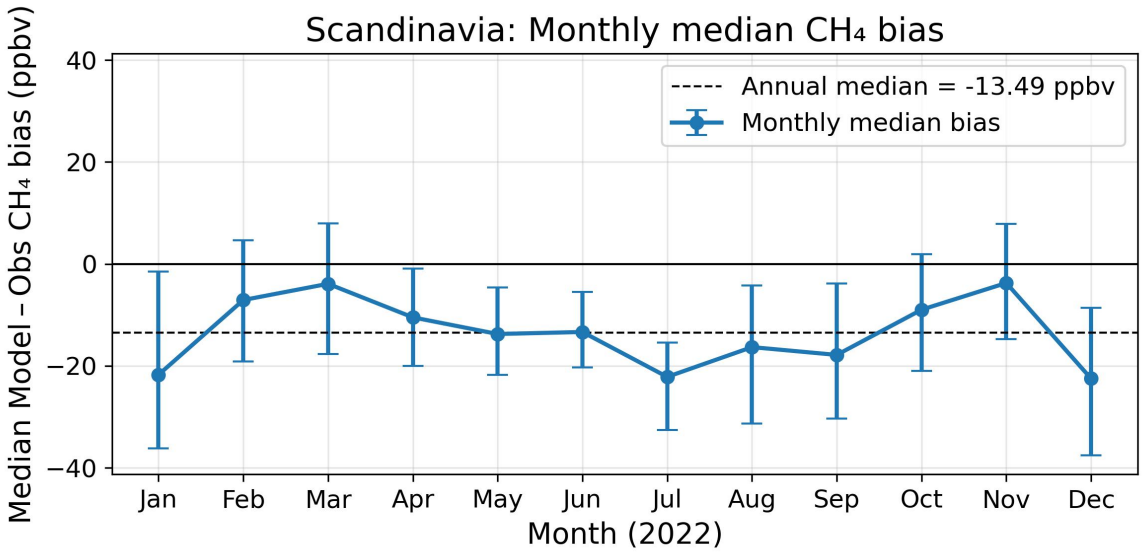

Figure 3.17.: Monthly median model–observation CH_4 bias for all stations in the 56–70° N, –10 to –34° E region during 2022. Markers show the monthly medians, the dashed line indicates the annual median bias (–13.49 ppbv), and the vertical bars span the interquartile range (25th–75th percentile).

Figure 3.17 shows that the monthly median bias, across all stations in this regional area, ranges from a minimum of about –21 ppbv (in January, July, and December) to a maximum of approximately –3 ppbv (in March and November), with an annual median of –13.49 ppbv. This consistent underprediction throughout 2022 suggests that the bias is a regional feature rather than unique to MHD. As we concluded from the Canadian latitude-band bias (fig. 3.11), the CAMS model possibly does not fully capture the seasonal OH decline during the darker months of the year. Additionally, in Scandinavia, pronounced underpredictions also occur during brighter months, which are likely linked to various modelling limitations of the CAMS framework. One large factor might be systematic errors in the anthropogenic fluxes, as those would be visible during all seasons, which also seem to influence MHD.

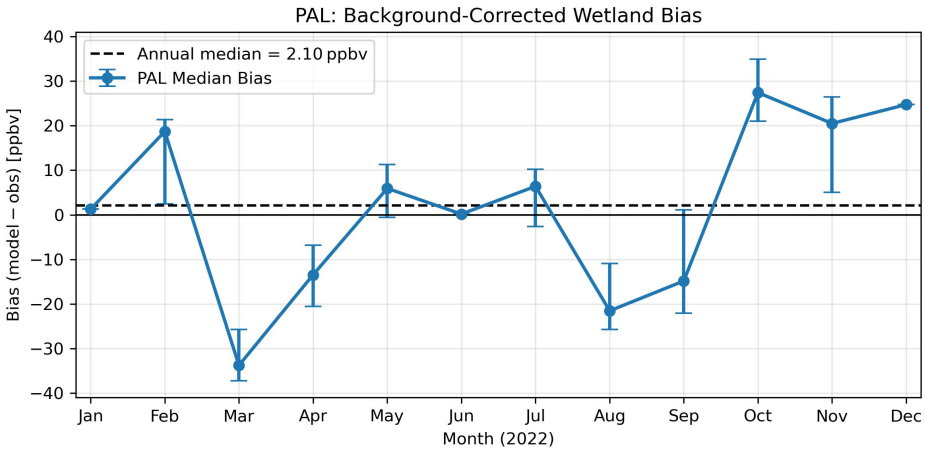

(a)

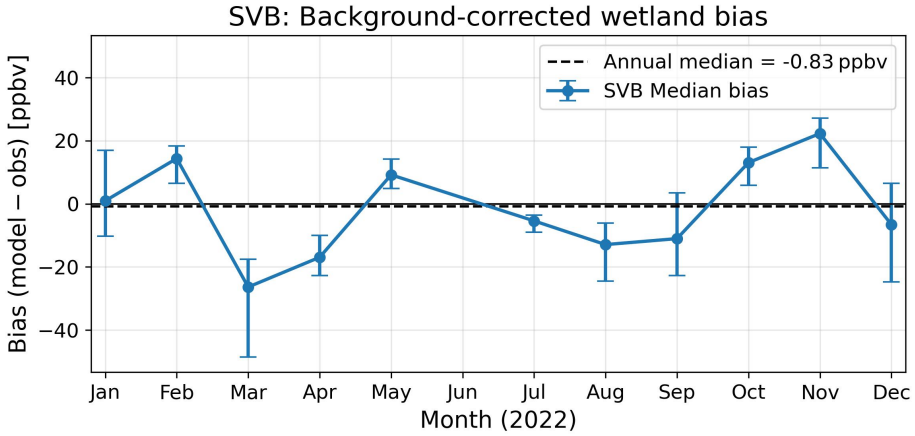

(b)

Figure 3.18.: Monthly median model–observation CH_4 bias after subtracting the Mace Head background station at Pallas (PAL, a) and Svartberg (SVB, b) for 2022. Markers show the background-corrected monthly medians, vertical bars span the interquartile range (25th–75th percentile) and the dashed line indicates the annual median bias (PAL: +2.1 ppbv; SVB: –0.83 ppbv).

In the background-corrected plots (fig. 3.18), the PAL median bias ranges from about –33 ppbv in March to +28 ppbv in October and an annual median of +2.1 ppbv. At SVB, the corrected bias ranges from –22 ppbv in March to +21 ppbv in November, averaging –0.83 ppbv over the year and there are no data for the month of June. However, we do not expect this data gap to have any influence on the observed bias pattern. In contrast to the Canadian wetland driven stations ETL and BCK, figure 3.18 shows a different seasonal

pattern for the two Scandinavian stations. Instead of the pronounced summer peak and lower values in winter, seen over Canada, both PAL and SVB exhibit a smoother, wave-shaped bias cycle. This is in alignment with our previous expectations, which suggest that anthropogenic and other non-wetland sources have very high influence on overall signal in Scandinavia [8, 39, 29]. Additionally, we found that the anthropogenic source contributions exhibit a seasonal pattern with increased winter emissions for both PAL and SVB (fig. 3.15). Thus, the positive bias during February, October and November might be explained by a systematic overestimation of the anthropogenic fluxes during those months. As there is only one datapoint for December at PAL, the overprediction there should be treated with caution. Additionally, this seasonal pattern is influenced by the subtraction of the MHD background, which imprints parts of its own variability onto the corrected PAL and SVB biases. Despite large deviations in some months (e.g., over -30 ppbv in March), the background corrected concentrations are very close to the observations, over the entire year (annual median bias < 2.2 ppbv), indicating that the model performs very well overall in Scandinavia.

Just as we did for the Canadian sites, we computed FLEXPART-derived monthly wetland contributions in ppbv for wetCHART, FLUXNET and Poulter et al. (2017) at the Scandinavian stations PAL and SVB, determined their deviations from the CAMS values, and added these (scenario–CAMS) differences to the background-corrected CAMS median biases from figure 3.18.

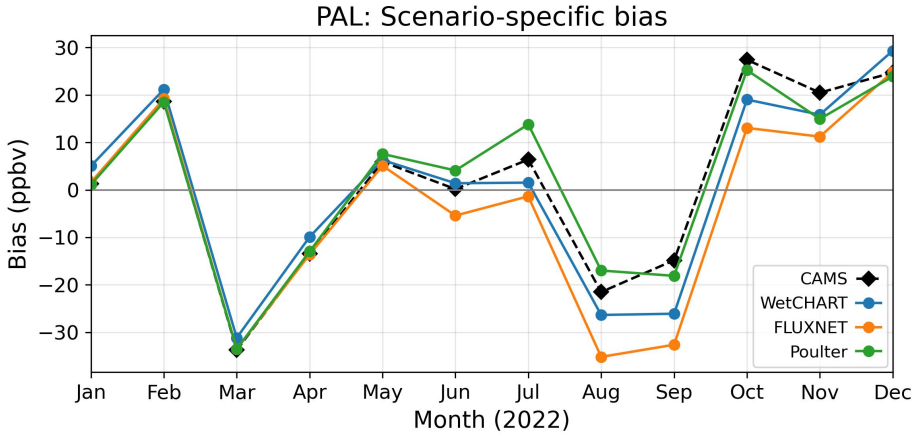

(a)

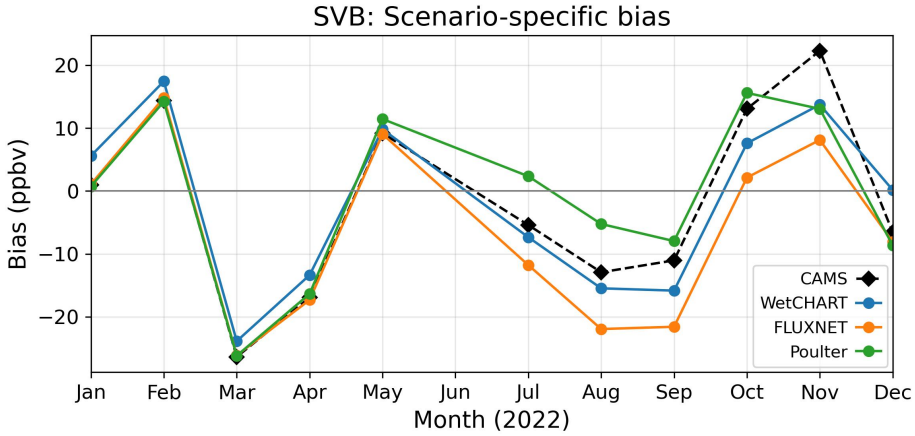

(b)

Figure 3.19.: Monthly background-corrected model–observation CH_4 median biases at (a) Pallas (PAL) and (b) Svartberg (SVB) for 2022. The dashed black lines show the CAMS reference bias, while the coloured lines show the scenario-specific biases for wetCHART, FLUXNET and Poulter et al. (2017), obtained by adding each monthly (scenario – CAMS) difference to the CAMS median bias.

Figure 3.19 shows that all three alternative scenarios reproduce CAMS's seasonal bias cycle at both PAL and SVB. In both panels, FLUXNET consistently produces the lowest biases throughout the year, whereas Poulter et al. (2017) yields the largest positive bias in summer yet otherwise remains very close to the CAMS reference through spring, autumn and winter, falling below CAMS in November. Lastly, wetCHART again overestimates in January and December, but otherwise closely follows CAMS, remaining

slightly below the reference from May to November. Here, FLUXNET and wetCHART exhibit the lowest annual median biases of only 0.11 ppbv and 0.15 ppbv for PAL and SVB, respectively.

However, unlike for Canada, where summers are overwhelmingly wetland dominated, in Scandinavia anthropogenic and other non-wetland sources contribute substantially to the emission landscape all year round. As a result, it is difficult to isolate a clear wetland bias from the background corrected comparison with measurements and we cannot confidently attribute parts of the positive or negative biases to uncertainties in wetland emission fluxes alone. Therefore, we cannot recommend specific wetland priors for future CH_4 concentration modelling in Scandinavia, as we did for Canada. A more detailed evaluation of the individual CAMS prior emission sources in Scandinavia is therefore required, to suggest model improvements for correcting the seasonally varying biases. This result for Scandinavia was expected, yet this example underscores the complexity of accurately modelling CH_4 emissions and reinforces the need for continued research to refine our understanding and representation of both wetland and non-wetland sources.

4. Conclusion and Outlook

In this thesis, we evaluated four wetland CH_4 scenarios: wetCHART, Poulter et al. (2017), FLUXNET-CH_4 and CAMS for 2018 (2017 for Poulter), with a focus on Canada and Scandinavia. These two boreal regions offer a combination of extensive wetlands and dense in situ measurements. Firstly, we examined flux fields of each scenario, to locate areas of consistently high emissions and detect model strengths and weaknesses. Subsequently, we calculated FLEXPART-footprints from stations in those high flux zones to quantify each sites sensitivity to wetland emissions. Additionally, we analysed, whether these stations are wetland dominated, or if anthropogenic emissions compete with wetland fluxes, by computing how much the wetland fluxes of the four scenarios, as well as the CAMS anthropogenic fluxes, contribute to each stations mixing ratio measurements in ppbv. Lastly, we compared CAMS concentration data to measurements (within the NOAA obspack datapackage) of the filtered stations, in order to assess their monthly biases. For Canada, we ultimately focused on the two wetland dominated stations East Trout Lake (ETL) and Behchoko (BCK) and used the Alert (ALT) site in Nunavut as our background reference station. In Scandinavia, we selected Pallas (PAL) and Svartberg (SVB) for the wetland bias analysis, and used Mace Head (MHD) on the west coast of Ireland as the continental background station.

Globally, all four wetland emission scenarios show the typical wetland CH_4 cycle: consistently high tropical fluxes year-round, near-zero boreal winter emissions and pronounced summer peaks in both hemispheres. However, they differ in spatial detail, seasonal amplitudes and coverage. WetCHART and the Poulter et al. ensemble both depict distinctly delineated wetland boundaries and generate the largest flux peaks over tropical and boreal areas. In contrast, CAMS diffuses localized hotspots into broader plumes, diluting peak fluxes across adjacent grid cells, representing the inherent smoothing in its 4D-Var inversion methodology. FLUXNET-CH_4 produces the least detailed emission maps and records the smallest peak fluxes.

Our model comparison clearly demonstrates the drastic differences among the four

wetland CH_4 scenarios. Canadian summer emission totals vary by up to ∼5 Tg, with FLUXNET-CH_4 estimating only about 30 % of Poulter et al. (2017), while CAMS and wetCHART estimate the second and third-highest emission, respectively. In Scandinavia, this order remains roughly the same, but the overall model differences are slightly less pronounced, while still yielding differences of around 50 % between the highest (Poulter) and the respective lowest estimates. Furthermore, we found that wetCHART overestimates winter fluxes by applying a constant temperature scaling, also across snow-covered areas, thereby neglecting the trapping of methane below the snowpack. These findings reveal the large uncertainties inherent in both bottom-up and top-down wetland emission models. We can therefore conclude that methane concentration fields generated using different wetland prior fluxes as input will yield substantially different results. We suggest that the choice of wetland priors should be optimised towards the best performing model within the respective study region.

The results from the background corrected CAMS concentration model-observation bias analysis, lead to vastly different conclusions for the two studied regions. For Canada, median model–observation biases at ETL and BCK remain near zero through winter and spring but rise sharply to +30 – +56 ppbv during the boreal summer, with annual medians of +8.7 ppbv at ETL and +28.7 ppbv at BCK. The strong seasonal cycle of these biases confirms that Canada's methane signal is heavily dominated by wetland emissions, which exceed the next largest source of anthropogenic emissions substantially. Therefore, this pronounced summer overprediction and relatively low bias during winter months, confirms that the CAMS wetland priors exceed observed CH_4 releases during the active wetland season. In this case, we conclude that wetland flux priors should be adapted to models that estimate lower emissions than the CAMS fluxes for the active season. From our scenario-specific bias analysis at the two Canadian stations, we suggest using either wetCHART, with an applied snow-cover mask to correct for the model not capturing snowpack trapping of methane, or FLUXNET. Although the latter exhibits negative biases at BCK and ETL during summer, its performance may differ at other Canadian sites. Since the other scenarios consistently overpredict summer emissions, FLUXNET-CH_4 stands out as a promising lower emission alternative to test on a wider range of Canadian wetland sites. We think that the major criterion should be the reduction of the overall regional bias, instead of focusing on regional details, because minimizing the aggregated bias in modelled concentrations ensures that the resulting CH_4 fields align most closely with observations, thereby addressing uncertainties in the global wetland methane budget. While station-based filtering allows us to isolate ideal,

wetland dominated sites and focus our bias analysis on those, the insights gained apply primarily to the immediate surroundings of ETL and BCK and should not be assumed to extend uniformly across all Canadian wetlands. As an avenue for future research we suggest using an ensemble of wetland dominated stations throughout Canada, instead of individual stations and test for a variety of wetland emission priors, which exhibit lower emissions than the CAMS fluxes. This methodology would reduce the overall noise in the data and allow for an assessment of the best performing wetland prior over a larger area, representing the broad wetland landscape in Canada. Furthermore, Liu et al. (2025) analysed a variety of process based models in Arctic and boreal North America and found that their divergence is driven more by uncertainties in soil carbon inventories and the wetland inundation extent than by temperature-sensitivity parameters [23]. Moreover, they concluded that the models LPJ-wsl and CLASSIC perform best out of all the examined models in relation to measurement data [25, 45, 23]. Hence, we propose also using these two models as prior flux fields for concentration data modelling and then following our suggested methodology for the bias analysis. Additionally, we also support the idea that future improvements of flux models in Canada should prioritize refining soil carbon inventories and implementing dynamic, high-resolution inundation mapping [23]. Of course, our recommended procedure is not limited to Canada, but only yields valuable results if wetlands heavily dominate the emission landscape. If there are other methane emission sources with comparable significance to wetlands, it is not trivial to isolate the influence of wetlands in the observed biases. Thus, one should not expect to be able to attribute seasonal patterns solely to wetlands.

This is the case for Scandinavia. Here, the background-corrected biases at PAL and SVB exhibit a wave shaped seasonal cycle rather than the sharp summer spike seen in Canada. Monthly medians swing between –33 and +28 ppbv at PAL and –22 and +21 ppbv at SVB, yet both stations yield annual medians close to zero (+2.1 ppbv and –0.8 ppbv, respectively). While a part of the positive biases during February, October and November likely stem from systematic overestimations of the anthropogenic priors, we can not confidently link positive or negative biases to wetland emission fluxes. In this region, emissions from multiple sources besides wetlands, such as livestock and waste, biomass burning or releases from oil and gas extraction, contribute comparably significant throughout the year. Thus, isolating a wetland-only bias poses a big challenge. Nevertheless, the close, near-zero annual medians at PAL and SVB demonstrate that, despite its variety of sources with comparable emissions, the CAMS inversion data delivers remarkably accurate CH_4 concentrations across these stations. This outcome both

highlights the inherent complexity of accurately modelling methane emissions over large regions and underscores the potential for future research to refine our comprehension and representation of not only wetland, but also non-wetland sources.

Acronyms

ALT	Alert atmospheric monitoring station (Nunavut, Canada)
BCK	Behchoko atmospheric monitoring station (Northwest Territories, Canada)
CAMS	Copernicus Atmosphere Monitoring Service
ETL	East Trout Lake atmospheric monitoring station (Saskatchewan, Canada)
FRD	Fraserdale boreal forest monitoring station (Ontario, Canada)
CARDAMOM	CARbon DAta MOdel fraMework inversion
NCEP	National Centers for Environmental Prediction
CRU	Climate Research Unit
GLWD	Global Lakes and Wetlands Database
LPJ-wsl	Lund–Potsdam–Jena Dynamic Global Vegetation Model (DGVM) (wsl - Wald Schnee Landschaft component)
ESA-GLOBCOVER	European Space Agency - global land cover product
MACE HEAD (MHD)	Mace Head atmospheric monitoring station (Ireland)
MERRA2	Modern-Era Retrospective analysis for Research and Applications, version 2
NOAA	National Oceanic and Atmospheric Administration
Obspack	NOAA observational data package
PAL	Pallas atmospheric observation station (Finland)
Poulter	Poulter et al. (2017) bottom-up wetland CH_4 flux data product
PUI	Puijo atmospheric monitoring station (Finland)
SWAMPS	Surface Water Microwave Product Series inundation dataset
TM5	A Transport–Chemistry model version 5
SVB	Svartberget atmospheric monitoring station (Sweden)
ECMWF	European Centre for Medium-Range Weather Forecasts
ERA5(-Land)	Fifth-generation ECMWF Reanalysis datasets (land component)

A. SI

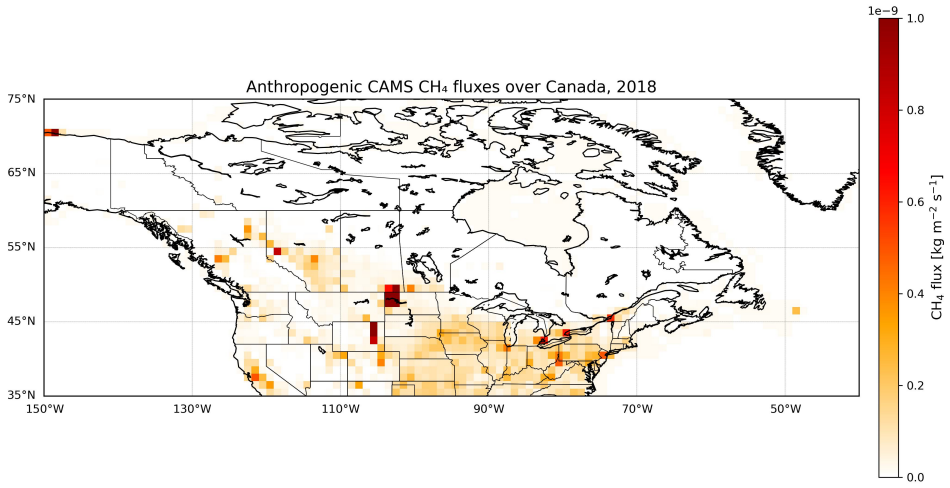

(a)

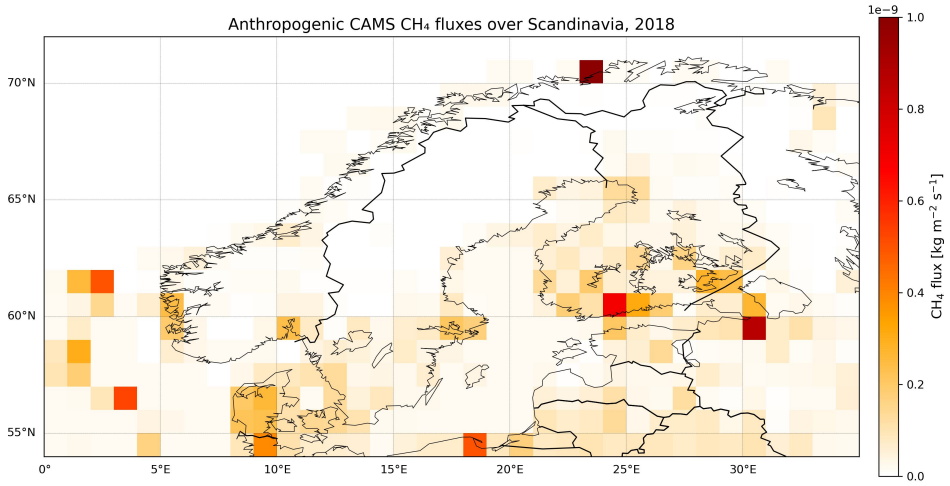

(b)

Figure A.1.: The Annual mean of the anthropogenic emission prior CH_4 fluxes, used by CAMS for 2018 in kg/m^{2}s over Canada (a) and Scandinavia (b). The colour bar is capped at 1e-9 kg/m^{2}s to highlight mid to low emission regions.

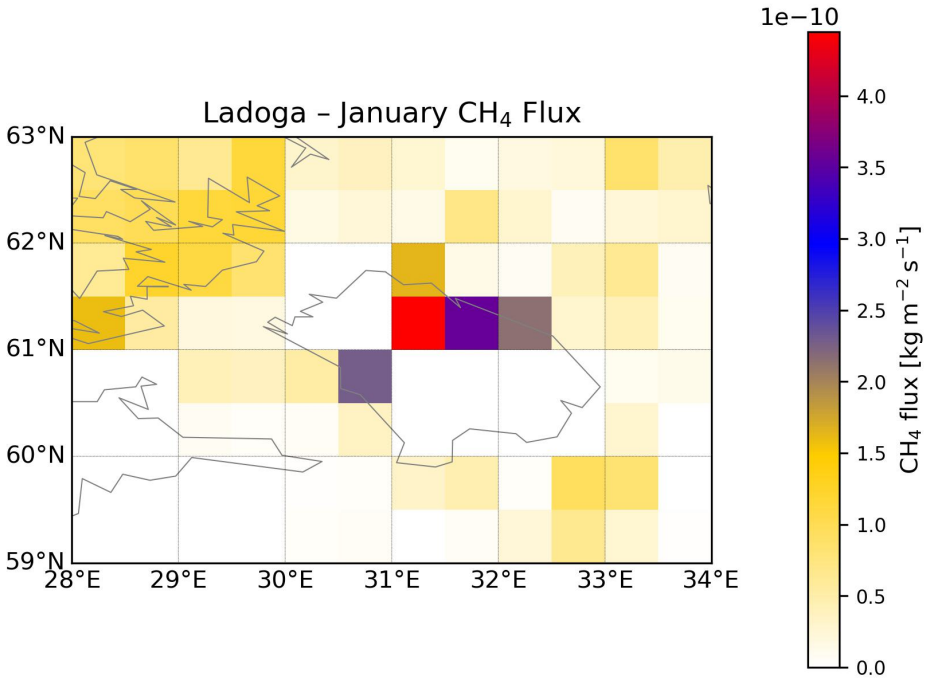

(a)

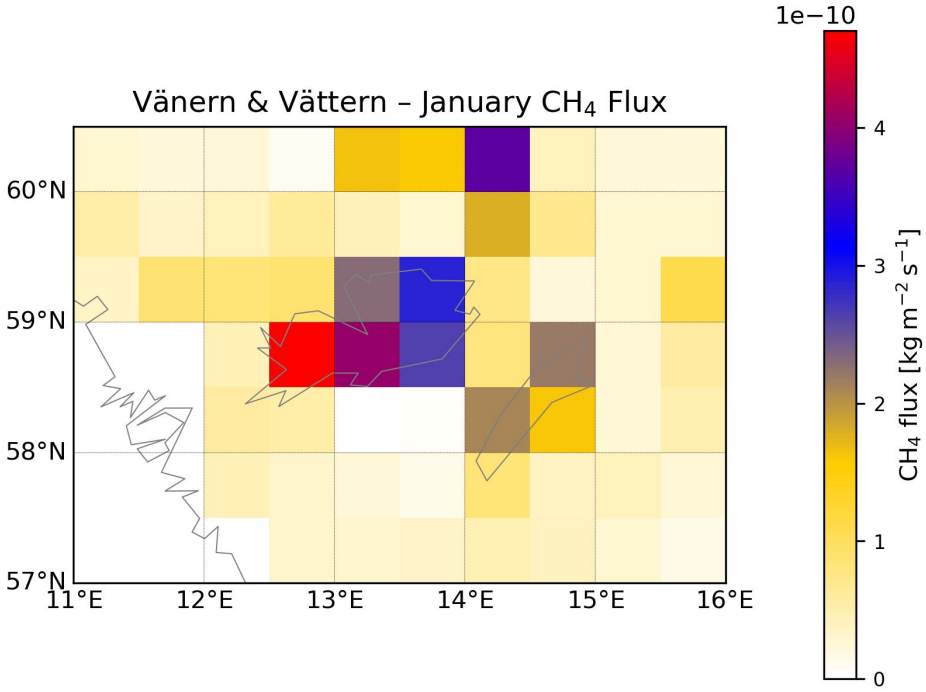

(b)

Figure A.2.: January wetCHART CH_4 fluxes in kg/m^{2}s over Lake Ladoga (a) and Lakes Vänern and Vättern (b). Emission pixels appear both around and within the frozen lake surfaces, likely resulting from inaccuracies in the used wetland mask or too coarse model resolution.

List of Figures

List of Tables

Bibliography

[1] Roger Atkinson and Janet Arey. Atmospheric degradation of volatile organic compounds. *Chemical reviews*, 103(12):4605–4638, 2003.

[2] Lucie Bakels, Daria Tatsii, Anne Tipka, Marina Dütsch, Michael Blaschek, Silvia Bucci, Andreas Plach, Martin Vojta, Petra Seibert, Ignacio Pisso, et al. Flexpart-11: Advancements in a lagrangian atmospheric model for enhanced accuracy, efficiency, and flexibility. Technical report, Copernicus Meetings, 2024.

[3] Sabour Baray, Daniel J Jacob, Joannes D Massakkers, Jian-Xiong Sheng, Melissa P Sulprizio, Dylan BA Jones, Anthony Bloom, and Robert McLaren. Estimating 2010–2015 anthropogenic and natural methane emissions in canada using eccc surface and gosat satellite observations. *Atmospheric Chemistry and Physics Discussions*, 2021:1–40, 2021.

[4] Peter Bergamaschi, Sander Houweling, Arjo Segers, M Krol, Christian Frankenberg, RA Scheepmaker, Edward Dlugokencky, Steven C Wofsy, EA Kort, Colm Sweeney, et al. Atmospheric ch4 in the first decade of the 21st century: Inverse modeling analysis using sciamachy satellite retrievals and noaa surface measurements. *Journal of Geophysical Research: Atmospheres*, 118(13):7350–7369, 2013.

[5] Peter Bergamaschi, Ute Karstens, Alistair J Manning, Marielle Saunois, Aki Tsuruta, Antoine Berchet, Alexander T Vermeulen, Tim Arnold, Greet Janssens-Maenhout, Samuel Hammer, et al. Inverse modelling of european ch 4 emissions during 2006–2012 using different inverse models and reassessed atmospheric observations. *Atmospheric Chemistry and Physics*, 18(2):901–920, 2018.

[6] Anthony Bloom, Kevin W Bowman, Meemong Lee, Alexander J Turner, Ronny Schroeder, John R Worden, Richard Weidner, Kyle C McDonald, and Daniel J Jacob. A global wetland methane emissions and uncertainty dataset for atmospheric chemical transport models (wetcharts version 1.0). *Geoscientific Model Development*, 10(6):2141–2156, 2017.

[7] Anthony Bloom, KW Bowman, M Lee, AJ Turner, R Schroeder, JR Worden, RJ Weidner, KC McDonald, and DJ Jacob. Cms: global 0.5-deg wetland methane emissions and uncertainty (wetcharts v1. 3.1). *ORNL DAAC*, 2021.

[8] Ingrid Bonde, Johan Kuylenstierna, Karin Bäckstrand, Katarina Eckerberg, Tomas Kåberger, Åsa Löfgren, Markku Rummukainen, and Sverker Sörlin. 2020: report of the swedish climate policy council, 2020.

[9] Scott D Bridgham, Hinsby Cadillo-Quiroz, Jason K Keller, and Qianlai Zhuang. Methane emissions from wetlands: biogeochemical, microbial, and modeling perspectives from local to global scales. *Global change biology*, 19(5):1325–1346, 2013.

[10] Kendra Couling. Identification of wetlands on the canadian boreal plain and their contributions to stream water chemistry, 2006.

[11] Kyle B Delwiche, Sara Helen Knox, Avni Malhotra, Etienne Fluet-Chouinard, Gavin McNicol, Sarah Feron, Zutao Ouyang, Dario Papale, Carlo Trotta, Eleonora Canfora, et al. Fluxnet-ch4: A global, multi-ecosystem dataset and analysis of methane seasonality from freshwater wetlands. *Earth System Science Data Discussions*, 2021:1–111, 2021.

[12] Yu A Fedorov and NS Tambieva. Methane formation and distribution in water and bottom sediments polluted by the pulp mill effluents (lake ladoga as an example). *Russian Meteorology and Hydrology*, (7):33–42, 2000.

[13] J.-L. France, A. Gorchov Negrón, J. Pitt, et al. Quantification and assessment of methane emissions from offshore oil and gas facilities on the norwegian continental shelf. *Atmospheric Chemistry and Physics*, 22:4303–4320, 2022. Includes aircraft-derived CH fluxes from Snøhvit, Goliat and 19 other offshore installations.

[14] Global Energy Monitor. Global Oil and Gas Extraction Tracker. `https://globalenergymonitor.org/projects/global-oil-gas-extraction-tracker/`, February 2025. February 2025 Release. Licensed under CC BY 4.0 International.

[15] Hans Hersbach, Bill Bell, Paul Berrisford, Shoji Hirahara, András Horányi, Joaquín Muñoz-Sabater, Julien Nicolas, Carole Peubey, Raluca Radu, Dinand Schepers, et al. The era5 global reanalysis. *Quarterly journal of the royal meteorological society*, 146(730):1999–2049, 2020.

[16] S Gerard Jennings, Christoph Kleefeld, Colin D O Dowd, Carsten Junker, T Gerard Spain, Phillip O Brien, Aodhaghan F Roddy, and Thomas C O Connor. Mace head atmospheric research station-characterization of aerosol radiative parameters. *Boreal environment research*, 8(4):303–314, 2003.

[17] Sari Juutinen, Jukka Alm, Tuula Larmola, Jari T Huttunen, Micaela Morero, Pertti J Martikainen, and Jouko Silvola. Major implication of the littoral zone for methane release from boreal lakes. *Global biogeochemical cycles*, 17(4), 2003.

[18] Sari Juutinen, M Rantakari, P Kortelainen, JT Huttunen, T Larmola, J Alm, J Silvola, and PJ Martikainen. Methane dynamics in different boreal lake types. *Biogeosciences*, 6(2):209–223, 2009.

[19] Gavin Kennedy and Tatiana Mayer. Natural and constructed wetlands in canada: An overview. *Water Quality Research Journal*, 37(2):295–325, 2002.

[20] Ernest N Koffi, Peter Bergamaschi, Romain Alkama, and Alessandro Cescatti. An observation-constrained assessment of the climate sensitivity and future trajectories of wetland methane emissions. *Science Advances*, 6(15):eaay4444, 2020.

[21] OR Kotsyurbenko, MV Glagolev, AY Merkel, AF Sabrekov, and IE Terentieva. Methanogenesis in soils, wetlands, and peat. *Biogenesis of hydrocarbons*, pages 211–228, 2019.

[22] Jean Le Mer and Pierre Roger. Production, oxidation, emission and consumption of methane by soils: a review. *European journal of soil biology*, 37(1):25–50, 2001.

[23] Gang Liu, Lu Shen, Philippe Ciais, Xin Lin, Didier Hauglustaine, Xin Lan, Alexander J Turner, Yi Xi, Yu Zhu, and Shushi Peng. Trends in the seasonal amplitude of atmospheric methane. *Nature*, pages 1–6, 2025.

[24] Yang Liu, Xiaokun Yao, Li Zhou, Tingzhen Ming, Wei Li, and Renaud de Richter. Removal of atmospheric methane by increasing hydroxyl radicals via a water vapor enhancement strategy. *Atmosphere*, 15(9):1046, 2024.

[25] Joe R Melton, Vivek K Arora, Eduard Wisernig-Cojoc, Christian Seiler, Matthew Fortier, Ed Chan, and Lina Teckentrup. Classic v1. 0: the open-source community successor to the canadian land surface scheme (class) and the canadian terrestrial ecosystem model (ctem)–part 1: Model framework and site-level performance. *Geoscientific Model Development*, 13(6):2825–2850, 2020.

[26] William J Mitsch, James G Gosselink, Li Zhang, and Christopher J Anderson. *Wetland ecosystems*. John Wiley & Sons, 2009.

[27] J. Muñoz Sabater. ERA5-Land monthly averaged data from 1950 to present. Copernicus Climate Change Service (C3S) Climate Data Store (CDS), 2019. Accessed on 20-May-2025.

[28] Intergovernmental Panel on Climate Change. Climate change 2014: Synthesis report. 2014.

[29] Mike Peacock, Martyn N Futter, William Lidberg, Mattias Lundblad, and Pia Geranmayeh. An upscaling of methane emissions from swedish flooded land. *Carbon Management*, 16(1):2445254, 2025.

[30] Norbert Pirk, Mikkel P Tamstorf, Magnus Lund, Mikhail Mastepanov, Stine H Pedersen, Maria R Mylius, Frans-Jan W Parmentier, Hanne H Christiansen, and Torben R Christensen. Snowpack fluxes of methane and carbon dioxide from high arctic tundra. *Journal of Geophysical Research: Biogeosciences*, 121(11):2886–2900, 2016.

[31] Ignacio Pisso, Espen Sollum, Henrik Grythe, Nina I Kristiansen, Massimo Cassiani, Sabine Eckhardt, Delia Arnold, Don Morton, Rona L Thompson, Christine D Groot Zwaaftink, et al. The lagrangian particle dispersion model flexpart version 10.4. *Geoscientific Model Development*, 12(12):4955–4997, 2019.

[32] Benjamin Poulter, Philippe Bousquet, Josep G Canadell, Philippe Ciais, Anna Peregon, Marielle Saunois, Vivek K Arora, David J Beerling, Victor Brovkin, Chris D Jones, et al. Global wetland contribution to 2000–2012 atmospheric methane growth rate dynamics. *Environmental Research Letters*, 12(9):094013, 2017.

[33] Michael J Prather, Christopher D Holmes, and Juno Hsu. Reactive greenhouse gas scenarios: Systematic exploration of uncertainties and the role of atmospheric chemistry. *Geophysical Research Letters*, 39(9), 2012.

[34] Celia J Sapart, G Monteil, Markella Prokopiou, Roderik SW van de Wal, Jed O Kaplan, P Sperlich, KM Krumhardt, C Van der Veen, S Houweling, MC Krol, et al. Natural and anthropogenic variations in methane sources during the past two millennia. *Nature*, 490(7418):85–88, 2012.

[35] Marielle Saunois, Ann R Stavert, Ben Poulter, Philippe Bousquet, Joseph G Canadell, Robert B Jackson, Peter A Raymond, Edward J Dlugokencky, Sander Houweling, Prabir K Patra, et al. The global methane budget 2000–2017. *Earth System Science Data Discussions*, 2019:1–136, 2019.

[36] Kenneth N Schuldt, Tuula Aalto, Aoki Arlyn Andrews, Apadula Shuji, Jgor Arduini Francesco, Sabrina Arnold, Bianca Baier, Jakub Bartyzel, Peter Bergamaschi, Tobias Biermann, et al. Multi-laboratory compilation of atmospheric carbon dioxide data for the period 1983-2021; obspack_ch4_1_globalviewplus_v5. 1_2023-03-08. *(No Title)*, 2023.

[37] P Seibert and A Frank. Source-receptor matrix calculation with a lagrangian particle dispersion model in backward mode. *Atmospheric Chemistry and Physics*, 4(1):51–63, 2004.

[38] Saurabh Sonwani and Pallavi Saxena. Introduction to greenhouse gases: Sources, sinks and mitigation. In *Greenhouse Gases: Sources, Sinks and Mitigation*, pages 1–7. Springer, 2022.

[39] Maria K Tenkanen, Aki Tsuruta, Hugo Denier van der Gon, Lena Höglund-Isaksson, Antti Leppänen, Tiina Markkanen, Ana Maria Roxana Petrescu, Maarit Raivonen, Hermanni Aaltonen, and Tuula Aalto. Partitioning anthropogenic and natural methane emissions in finland during 2000–2021 by combining bottom-up and top-down estimates. *Atmospheric Chemistry and Physics*, 25(4):2181–2206, 2025.

[40] Merritt R Turetsky, Agnieszka Kotowska, Jill Bubier, Nancy B Dise, Patrick Crill, Ed RC Hornibrook, Kari Minkkinen, Tim R Moore, Isla H Myers-Smith, Hannu Nykänen, et al. A synthesis of methane emissions from 71 northern, temperate, and subtropical wetlands. *Global change biology*, 20(7):2183–2197, 2014.

[41] Den Volokin and Lark ReLlez. On the average temperature of airless spherical bodies and the magnitude of earth's atmospheric thermal effect. *SpringerPlus*, 3(1):723, 2014.

[42] RJE Vroom, M Van Den Berg, SR Pangala, OE Van Der Scheer, and BK Sorrell. Physiological processes affecting methane transport by wetland vegetation–a review. *Aquatic Botany*, 182:103547, 2022.

[43] Sophie Wittig, Antoine Berchet, Isabelle Pison, Marielle Saunois, Joël Thanwerdas, Adrien Martinez, Jean-Daniel Paris, Toshinobu Machida, Motoki Sasakawa, Douglas EJ Worthy, et al. Estimating methane emissions in the arctic nations using surface observations from 2008 to 2019. *Atmospheric Chemistry and Physics*, 23(11):6457–6485, 2023.

[44] Zhen Zhang, Benjamin Poulter, Joe R Melton, William J Riley, George H Allen, David J Beerling, Philippe Bousquet, Josep G Canadell, Etienne Fluet-Chouinard, Philippe Ciais, et al. Ensemble estimates of global wetland methane emissions over 2000–2020. *Biogeosciences*, 22(1):305–321, 2025.

[45] Zhen Zhang, Niklaus E Zimmermann, Leonardo Calle, George Hurtt, Abhishek Chatterjee, and Benjamin Poulter. Enhanced response of global wetland methane emissions to the 2015–2016 el niño-southern oscillation event. *Environmental Research Letters*, 13(7):074009, 2018.